HHS Public Access

Author manuscript

Cell Rep. Author manuscript; available in PMC 2023 August 20.

Published in final edited form as:

Cell Rep. 2023 July 25; 42(7): 112723. doi:10.1016/j.celrep.2023.112723.

Proteins rather than mRNAs regulate nucleation and persistence of Oskar germ granules in *Drosophila*

Harrison A. Curnutte[1,2], **Xinyue Lan**[1,2], **Manuel Sargen**[1,2], **Si Man Ao Ieong**[1], **Dylan Campbell**[1], **Hyosik Kim**[1], **Yijun Liao**[1], **Sarah Bailah Lazar**[1], **Tatjana Trcek**[1,3,*]

[1]Department of Biology, Johns Hopkins University, 3400 N. Charles Street, Baltimore, MD 21218, USA

[2]These authors contributed equally

[3]Lead contact

SUMMARY

RNA granules are membraneless condensates that provide functional compartmentalization within cells. The mechanisms by which RNA granules form are under intense investigation. Here, we characterize the role of mRNAs and proteins in the formation of germ granules in *Drosophila*. Super-resolution microscopy reveals that the number, size, and distribution of germ granules is precisely controlled. Surprisingly, germ granule mRNAs are not required for the nucleation or the persistence of germ granules but instead control their size and composition. Using an RNAi screen, we determine that RNA regulators, helicases, and mitochondrial proteins regulate germ granule number and size, while the proteins of the endoplasmic reticulum, nuclear pore complex, and cytoskeleton control their distribution. Therefore, the protein-driven formation of *Drosophila* germ granules is mechanistically distinct from the RNA-dependent condensation observed for other RNA granules such as stress granules and P-bodies.

Graphical abstract

*Correspondence: ttrcekp1@jhu.edu.

AUTHOR CONTRIBUTIONS

Conceptualization, T.T.; methodology, H.A.C. and T.T.; investigation and analysis, H.A.C., X.L., M.S., S.M.A.I., D.C., H.K., Y.L., S.B.L., and T.T.; writing – original draft, H.A.C. and T.T.; writing – review & editing, funding acquisition, resources, and supervision, T.T.

SUPPLEMENTAL INFORMATION

Supplemental information can be found online at https://doi.org/10.1016/j.celrep.2023.112723.

DECLARATION OF INTERESTS

The authors declare no competing interest.

INCLUSION AND DIVERSITY

We support inclusive, diverse, and equitable conduct of research.

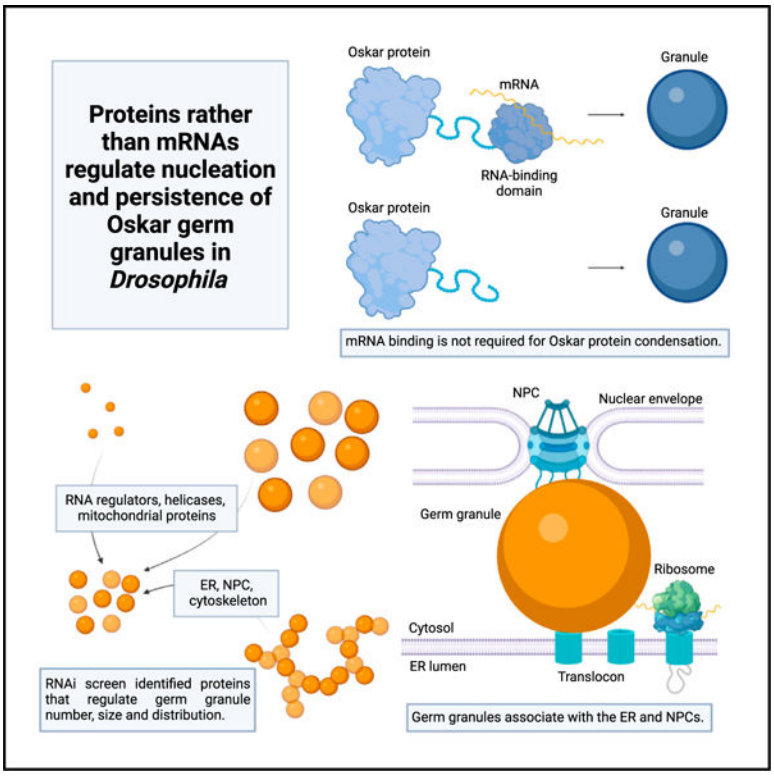

In brief

Curnutte et al. observe that germ granule proteins rather than mRNAs promote the nucleation and stability of Oskar germ granules in *Drosophila*. While RNA regulators and mitochondrial proteins control the number and size of germ granules, the proteins of the ER, nuclear pores, and cytoskeleton control their distribution.

INTRODUCTION

RNA granules compartmentalize and concentrate RNA regulators and RNAs in cells. They are inextricably linked to post-transcriptional gene regulation and associated with human diseases.[1] Some RNA granules, such as stress granules, which accumulate RNAs during cellular stress, and processing bodies (P-bodies), which are linked to mRNA degradation, are ubiquitous and form in all cells. Other RNA granules, namely germ granules, which instruct the germ cell fate, form in specialized cells. RNA granules often form in distinct cellular locations. This creates asymmetries in protein and RNA concentrations, which polarize cells both in shape and function. In addition, RNA granules are thought to promote inter- and intra-molecular interactions that may enhance biological reactions required for cell growth and development.[2] Given the benefits that RNA granules appear to provide to a cell, it is important to understand the mechanisms that govern their formation.

RNA granules form by phase separation, a process that promotes condensation of granule components into larger, non-membrane-bound, and mostly spherical condensates. Weak, multivalent interactions among granule components are critical for the formation of

granules. They give rise to a dynamic network that endows RNA granules with liquid-like properties. These properties allow RNA granules to condense and dissolve quickly in response to cellular and environment signals and exchange components with their surroundings.[3]

Proteins that reside in granules tend to contain low complexity domains (LCDs) and intrinsically disordered regions (IDRs), which promote protein condensation.[3,4] In addition, RNA-binding proteins (RBPs), protein chaperones, heat shock proteins, protein degradation factors, and post-translational modifications regulate protein condensation.[5–7]

Interestingly, RNA has emerged as an important regulator of the formation and persistence of RNA granules, including stress granules, P-bodies, the mammalian TIS granules, the Whi3 granules in *Ashbya gossypii*, glycolytic bodies in *Saccharomyces cerevisiae*, and P granules (the germ granules in *Caenorhabditis elegans*).[5,8–16] RNAs are thought to achieve this feat by engaging in many protein:RNA and RNA:RNA interactions, thus providing a scaffold for the condensation of granule proteins.[17,18] Not surprisingly, RNA helicases are common constituents of RNA granules,[7,19] where they are thought to dissolve RNA:RNA interactions to limit condensation and growth of RNA granules.[20]

In *Drosophila*, germ granules form in a specialized cytoplasm called germ plasm, which accumulates at the posterior of the late oocyte and early embryo. There, germ granules are thought to regulate translation and decay of a subset of mRNAs necessary for the establishment of primordial germ cells (PGCs).[21–24] Removal of the germ plasm prevents the formation of PGCs and abolishes embryonic patterning,[25–27] underscoring the observation that germ plasm and its germ granules are required for the development of the fly.

The *Drosophila* germ granules are nucleated by Oskar (Osk),[21,25,28] a protein encoded by an mRNA, which localizes to the posterior during mid oogenesis. Multiple mechanisms localize *oskar* (*osk*) mRNA. Initially, dynein-mediated transport delivers it from the nurse cells into oocyte. Afterward, kinesin motors help enrich it at the posterior, and the RNA localization element that forms during splicing of *osk*[29] is required for this transport.[30] In addition, translation of *osk* is repressed during transport and relieved only at the posterior,[31,32] which ensures that germ granules form at the correct time and place. Afterward, Osk recruits other granule components, including Vasa, a conserved DEAD-box RNA helicase; Tudor (Tud), a Tudor-domain protein required for protein:protein interactions; and Aubergine (Aub), an Argonaute family protein involved in piRNA biosynthesis.[27] Osk is also an RBP predicted to bind germ granule mRNAs, including *nanos* (*nos*), *polar-granule-component* (*pgc*), *germ cell less* (*gcl*), and *CycB*.[33,34]

Once germ granules form, filamentous (F) actin and cortical microtubules enable sustained anchoring of germ granules,[28,35–38] which keeps them enriched at the posterior. Indeed, fully functional germ granules persist for several hours when fertilization is delayed.[39,40] In addition, germ granules display liquid and hydrogel-like properties[26] that are thought to promote biological reactions in germ granules and allow germ granules to resist dissolution during purification.[26] However, apart from Osk and a few other factors, little is known about

how components, resident to germ granules, instruct the formation and the stability of the *Drosophila* germ granules.

Here, we employed quantitative, super-resolution microscopy to identify mechanistic principles that govern the formation of germ granules in the fly. Surprisingly, we find that, while RNA controls the size and composition of germ granules, it is not required for their nucleation and persistence. Instead, an RNAi screen identified 30 genes that regulate the number, size, and distribution of germ granules, 25 of which have not been previously described in this role. Therefore, we demonstrate that the formation of the *Drosophila* germ granules is primarily driven by proteins in a process that is mechanistically distinct from the RNA-dependent condensation typically observed for RNA granules.

RESULTS

The number, size, and distribution of germ granules are precisely controlled

To identify factors that control the formation of germ granules in *Drosophila*, we first determined how their number, size, and distribution changed during their life cycle. We focused our studies on the germ granule nucleator Osk, since changes in the accumulation of this protein best reflect the spatiotemporal changes of germ granules.[21,28] To visualize germ granules *in vivo*, we used flies in which the endogenous *osk* locus was tagged with GFP (Osk:GFP) by CRISPR-Cas9 genome editing. These flies had egg hatching rates similar to wild-type (WT) flies (Figure S1A), indicating that Osk:GFP retained WT function and formed functional germ granules.

We began our measurements at oogenic stage 10A, the time when germ granules and their mRNAs begin to accumulate at the posterior of the developing oocyte,[38,41,42] and finished at nuclear cycle (NC) 14 of the early embryo, when most germ granules disappear.[26] To count Osk:GFP granules, we used a spot detection algorithm[43,44] and observed that granules accumulated in four distinct phases (Figures 1A–1C). During the first phase, which lasted approximately 9 h and encompassed oogenic stages 10A and 10B, 31.0% of Osk:GFP granules were formed. During the second phase, which included oogenic stages 11 and 12, 50.3% of Osk:GFP granules formed in less than 3 h. With the onset of the third phase during oogenic stage 13, granule formation slowed and reached a peak several hours later in embryogenesis during NC 1–8. Finally, during the fourth phase, which took place after NC 8, the number of germ granules began to decrease until late NC 14, when only 16.0% of Osk:GFP granules could be detected at the posterior (Figures 1B and 1C). Live imaging revealed that germ granules are anchored and largely immobile at the posterior.[45] Furthermore, fluorescence recovery after photo bleaching (FRAP) analysis demonstrated that Osk:GFP granules exchange less than 40% of their content with the surrounding cytoplasm.[26] These published results combined with our data (Figure 1C) indicate that germ granules maintain their numbers because they are remarkably persistent rather than being replenished by continuous dissolution and condensation of Osk protein.

With a diameter of 250 nm,[46] individual germ granules are not much bigger than the resolution limit of our structured illumination microscope (SIM),[47] which prevented us from reliably recording decreases in the physical size of germ granules. Instead, to estimate

changes in germ granule size, we measured the intensity of Osk:GFP fluorescence per granule, which reflected the abundance of Osk protein per granule and hence its size (STAR Methods). Using this approach, we recorded that germ granule size fluctuated during development (Figure 1D). Initially, granule size increased slightly until oogenic stage 13, after which it began to diminish until NC 14, when only 20.2% of Osk:GFP fluorescence per granule remained (Figure 1D). However, as the total amount of Osk:GFP fluorescence at the posterior increased by 4.6-fold between oogenic stage 10 and 13 (Figures S1B and S1C), the average size of Osk:GFP granules increased by only 1.1-fold (Figure 1D). Instead, new granules formed, spanning an ever-increasing area at the posterior (Figures 1E, S1D, and S1E). Thus, Osk:GFP granules have a finite size that, when reached, triggers the formation of additional new granules rather than promoting growth of increasingly bigger ones.

Importantly, as new germ granules formed, their number per square micrometer (μm^2) did not change throughout oogenesis (Figure 1E). These data revealed that the spatial distribution of germ granules and therefore their anchors at the posterior is controlled during development. Moreover, the 1.6 to 1.8 germ granules per μm^2 we recorded using SIM and spot detection analysis was the same as the previous results of 1.7 germ granules per μm^2 recorded by electron microscopy (EM).[41] This result indicated that our methods identified individual, well-separated germ granules. After NC 9, however, germ granules became organized into crescents surrounding the nuclei of the future PGCs (Figure 1Biv), consistent with previous observations.[48] These granules are coupled to astral microtubules, giving rise to the crescent organization of germ granules among dividing PGCs.[48]

Furthermore, the number and size of Osk:GFP granules closely followed the accumulation of *osk* mRNA and total Osk:GFP protein at the posterior (Figures S1B and S1C), in agreement with previous observations.[38,42] Thus, changes in the number and size of Osk:GFP granules can be largely explained by the amount of localized and translating *osk* mRNA, the stability of Osk protein, and its ability to condense into granules.

Notably, we observed similar spatiotemporal changes in the accumulation of germ granules labeled with the Vasa:GFP protein generated by CRISPR-Cas9 genome editing (Figure S1F and S1G). This was an anticipated result given that Osk and Vasa interact with each other and that the accumulation of Vasa in germ granules depends on Osk.[26,49,50] In support of this observation, the FRAP kinetics of Vasa:GFP are similar to those recorded for Osk:GFP,[26] suggesting that the behavior of Vasa in granules is dictated by Osk. Finally, *nos*, *pgc*, and *CycB* mRNAs also accumulated in a manner similar to Osk:GFP (Figures 1F, 1G, and S1H), indicating that mRNA enrichment at the posterior depended on the amount of germ granule proteins, supporting previous observations.[42,43]

Together, our measurements revealed that the number, size, and distribution of germ granules are spatiotemporally controlled. To determine how this control is achieved, we set out to identify the factors that regulate the formation of germ granules.

Osk-bound mRNAs are not required for condensation of Osk protein

Many RNA granules rely on RNA for their formation. In contrast to these findings, Osk protein, which lacks its RNA-binding (SGNH) domain, forms granules efficiently when

expressed in *Drosophila* S2 cell lines.[26] These data indicate that the nucleation of the *Drosophila* germ granules does not require interaction of Osk protein with its mRNA. To address this possibility in the embryo, we ectopically expressed Osk, which lacked the SGNH domain (ΔSGNH Osk) and its full-length counterpart (FL Osk) at the anterior pole (Figure 2A), as previously described.[51] Tagging of the two Osk variants with the mCherry fluorescent protein allowed their detection.[51] Single-molecule fluorescent *in situ* hybridization (smFISH) analysis of nine germ granule mRNAs confirmed that only the expression of the FL Osk resulted in enrichment of mRNAs at the anterior pole (Figures 2B, 2C, S2A, and S2B). However, regardless of RNA-binding capacity, we observed that both FL Osk and ΔSGNH Osk formed granules (Figures 2B, 2C, S2A, and S2B), demonstrating that, in the embryo, Osk was able to condense without binding to the mRNA. Our results thus demonstrated that the nucleation of germ granules does not require Osk-bound mRNA.

RNA is required for composition but not persistence of germ granules

To determine whether RNA is required for the persistence of germ granules, we degraded RNAs in live oocytes with RNase A and investigated the effect of this treatment on germ granules. We used oocytes because we could deliver RNase A in them using a mild Triton X-100 treatment.

Our experiments revealed that a 30-min treatment of oocytes with RNase A did not dissolve Osk:GFP granules (Figures 3A and 3B). Instead, these oocytes displayed the same number of granules as those that were treated only with Triton or those that were immediately fixed upon dissection (‘‘untreated’’ sample) (Figure 3C). smFISH confirmed that *nos* and *osk* mRNAs were degraded in oocytes treated with RNase A but were still present in oocytes treated with Triton alone (Figures 3A and 3B). We verified these results with quantitative RT-PCR (qRT-PCR) analysis, which demonstrated that RNase A treatment reduced mRNA levels in the RNase A-treated oocytes by more than 99.9% compared with Triton-only treated oocytes (Figures S3A and S3B). Osk:GFP granules were observed in RNase A-treated oocytes across all oogenic stages (Figure S3Ci and S3Cii). Remarkably, even a 2-h treatment with RNase A did not dissolve Osk:GFP granules (Figure S3D). RNase A treatment also did not dissolve Vasa:GFP or Tud:GFP granules (Figure S3E) or reduce the amount of these proteins at the posterior (Figure S3F), but it did significantly reduce Aub:GFP signal (Figures S3E and S3F). Thus, unlike Osk:GFP, Vasa:GFP, and Tud:GFP, Aub:GFP requires RNA for its enrichment in germ granules. Finally, oocytes treated with RNase A formed 1.8-fold bigger granules compared with untreated oocytes (Figure 3D), indicating that RNA has a role in regulating the size of Osk:GFP granules.

However, the 1.3-fold increase in granule size upon Triton treatment (Figure 3D) raised a possibility that the detergent could have increased the stability of germ granules and counteracted the destabilizing effect that the removal of RNA in RNase A-treated oocytes might have had. To test this possibility, we isolated germ granules from NC 1–8 embryos using a detergent-free buffer and incubated isolated granules with RNase A or an RNase inhibitor. We observed that RNase A treatment did not dissolve isolated germ granules or change their appearance compared with granules treated with an RNase inhibitor (Figure S3G). qRT-PCR analysis confirmed that RNase A treatment reduced *nos*, *pgc*, and *CycB*

levels compared with the samples treated with RNase inhibitor by more than 99.9% (Figure S3H). In addition, denaturing agarose gel electrophoresis revealed that RNA was efficiently degraded in RNase A-treated samples (Figure S3I), further supporting our observation that the removal of RNA with RNase A was efficient.

Our results demonstrated that, while RNA limits incorporation of Osk:GFP into granules and thus their size, germ granules maintain their number and distribution upon removal of the RNA with RNase treatment over extended periods of time. Taken together, our data revealed that the nucleation and persistence of *Drosophila* germ granules relies primarily on germ granule proteins.

RNAi screen identifies regulators of germ granule number, size, and distribution

To identify proteins that are required for the formation of germ granules, we performed an RNAi screen of genes encoding the 117 proteins that have previously been co-immunoprecipitated with Osk.[51] These genes included the core germ granule constituents Vasa, Tud, and Aub and 114 additional proteins, whose function in the formation of germ granules is largely unclear. We reasoned that proteins resident to germ granules would have a high likelihood of regulating the properties of germ granules, including their number, size, and distribution.

To identify candidate genes that could regulate germ granules, we first evaluated the efficiency of gene expression knockdown (KD) of individual RNAi using qRT-PCR and egg hatching analysis. Afterward, we examined whether the expression of RNAi lines changed mRNA localization pattern at the posterior (Figure 4A). Given that the efficiency of mRNA localization correlated with the number of germ granules (Figures 1F, 1G, and S1H), we reasoned that any change in the levels of localized mRNAs could reflect a change in germ granule number, size, and distribution. Finally, we identified *bona fide* regulators of germ granules by investigating how the reduction of gene expression of candidate genes changed the number, size, and distribution of fluorescently labeled germ granules (Figure 4A). We focused on embryos during NC 1–8, since, at this developmental stage, aside from their size, the number and distribution of germ granules changed minimally compared with other developmental stages (Figures 1C–1E).

Individual RNAi-mediated KD of 117 genes was performed using the UAS-Gal4 system. The expression of the Gal4 inducer was driven by the promoter of the *maternal alpha tubulin* (*mat*a) gene, which restricted the expression of the RNAi to late oogenesis,[52] when germ granules begin to appear (Figure 1C). KD of 11 genes gave rise to females that did not lay eggs, while for 26 genes, RNAi reduced target mRNA expression by less than 35% (Figures 4A and S4A; Table S1), which allowed us to triage these genes from further analysis.

However, for 80 of the 117 genes, RNAi reduced target mRNA expression by more than 35%, with 46 of them reducing expression by more than 90% (Figure S4A; Table S1). Since many of these genes encoded essential proteins that are required for early embryonic development (Table S1), we reasoned that we could evaluate how efficiently these RNAi lines reduced protein expression by measuring the rate of egg hatching. We observed that, of the 80 genes that demonstrated KD efficiency greater than 35%, 47 of them demonstrated

a reduction in egg hatching rate greater than 50% (Figure S4B, magenta bars; Table S1). In contrast, only two of the 26 genes with KD efficiency less than 35% demonstrated a reduction in egg hatching rate greater than 50% (Figure S4B, black bars; Table S1). These data suggested that the RNAi lines we used efficiently reduced not only the mRNA levels of target genes but also of the proteins these mRNAs code for. Taken together, our qRT-PCR and egg hatching analysis identified 80 candidate genes suitable for further analysis.

We then examined the 80 candidate genes for their role in germ granule formation. We evaluated how their KDs changed the localization of *nos*, *pgc*, and *CycB* mRNAs to granules, as this approach allowed for a rapid screening of germ granule phenotypes with minimal genetic manipulation. We identified 37 candidate genes that altered mRNA localization pattern of *nos*, *pgc*, and *CycB*, while 43 of them displayed WT mRNA localization pattern of these genes (Figure 4A and S4C−S4F). KD of 26 of these 37 genes reduced or abolished mRNA localization, while KD of one gene, *Pgam5*, increased it (Figures S4C−S4E). Eighteen of these encoded for RBPs and 19 encoded non-RBPs (Figure S4D). We also identified 10 genes whose KD caused extensive branching of germ granules with a mesh-like appearance, which indicated that the distribution of granules was dysregulated in these embryos (Figures S4D−S4F, gene names in blue). KDs of four of these genes triggered only changes in the distribution of granules, while six also reduced the localization efficiency of *nos*, *pgc*, and *CycB* (Figure S4D and S4E).

We then sought to determine whether the 37 candidate genes were *bona fide* regulators of germ granule formation. To visualize granules, we crossed the flies that expressed RNAi with those expressing either Osk:GFP or Vasa:GFP, depending on the chromosomal integration of a particular RNAi construct (Figure 4A; Table S1). In this and our previous studies, we demonstrated that Vasa:GFP granules recapitulate all the principal features of Osk:GFP granules, including their number, size, distribution (Figures 1C–1E, S1F, and S1G), location, and biophysical properties.[26,43,44] Thus, we conclude that Vasa:GFP and Osk:GFP can be used interchangeably for the interrogation of germ granule properties.

Our analysis revealed that seven of the 37 candidate genes failed to display a germ granule phenotype (Figure 4A). These genes likely represented proteins required for mRNA enrichment to granules but not for the formation of germ granules. However, we identified 30 hit genes required for the formation of germ granules, 25 of which have not been previously characterized in this role. Importantly, these changes in germ granule number, size, and distribution were also observed in embryos that expressed WT Osk and Vasa (Figure S4C–F), demonstrating that GFP tagging of these two proteins did not trigger changes in the behavior of germ granules.

Of the 30 hit genes, we observed that 21 of them affected granule number (i.e., *Hrb98DE*) and size (i.e., *Pgam5*), while nine genes, including *Srp68*, affected granule distribution (Figure 4B). Interestingly, the genes that affected granule number, size, and distribution fell into two distinct groups (Figure 4C). Gene KDs that affected granule number and size were enriched for RNA regulators, helicases, and mitochondrial proteins, while those that affected granule distribution encoded proteins of the endoplasmic reticulum (ER), nuclear

pore complex (NPC), and cytoskeleton. We next characterized the phenotypes of genes belonging to these two groups.

RNA regulators, helicases, and mitochondria proteins control germ granule number and size

The number and size of germ granules depend on their stability and anchoring as well as the ability of Osk protein to condense and nucleate new granules. These steps depend on the abundance of Osk (Figures 1C–1E), which in turn relies on Osk protein stability as well as *osk* mRNA localization and translation.

We identified 21 genes whose KDs changed the number and size of granules (Table S1). We compared the phenotypes produced by the KD of these genes with those of *staufen* (*stau*), *valois* (*vls*), and *capsuleen* (*csul*). These three proteins did not co-purify with Osk[51] but are known regulators of Osk protein expression and germ plasm assembly.[53–55]

We observed that 10 of the 21 gens (*lark*, *Khc*, *CG2246*, *Klp3A*, *sub*, *Sec31*, *Mcm5*, *Hrb98DE*, *wisp*, *aub*) also reduced localization of *osk* mRNA (Figure S5A−S5E), suggesting that the primary function of these 10 genes in the formation of germ granules may be in regulating *osk* mRNA enrichment rather than in regulating the germ granules themselves.

However, KD of the remaining 11 genes (*vas*, *CG5641*, *CG7878*, *Usp7*, *eIF2α*, *Pagm5*, *Trap1*, *Nipped-A*, *Mcm3*, *tud*, *Pfas*) changed the number and size of granules without reducing localization of *osk* mRNA (Figure S5C). These genes encode splicing and translational regulators (*CG5641*, *eIF2α*), RNA helicases (*vas*, *CG7878*), DNA helicases and DNA repair proteins (*Mcm3*, *Nipped-A*), mitochondrial regulators and chaperones (*Trap1*, *Pagm5*), and proteins involved in the synthesis of purine nucleotides (*Pfas*) and protein turnover (*Usp7*) (Figure 5D). These proteins affected granules in three ways. The KD of *vas* and of *CG5641* reduced the number of granules by 48% and 56%, respectively, while increasing their size only by 15% and 25%, respectively (Figures 5Ai and 5Aii). Thus, if fusion among granules occurred, it moderately contributed to the decrease in the number of granules. Instead, *vas* and *CG5641* may regulate anchoring or stability of granules or limit the ability of Osk protein to nucleate granules.

The KD of *CG7878*, *Usp7*, *eIF2α*, and *Pgam5* did not affect the number of granules (Figure 5Bi) but instead affected their size (Figure 5Bii). Thus, in these embryos, granules nucleated and anchored efficiently and were stable but did not grow normally. Specifically, upon KD of *Pgam5*, embryos formed granules that were 55% larger than WT germ granules (Figure 5Bii), while over-expression (OE) of *Pgam5* (*Pgam5* OE) reduced their number and size by 77% and 17%, respectively (Figures S6Ai and S6Aii). Conversely, KDs of *CG7878*, *Usp7*, and *eIF2α* reduced granule size by 76% (*CG7878*) to 39% (*eIF2α*) (Figure 5Bii), suggesting that these genes likely regulated translation of *osk* mRNA, Osk protein stability, or its ability to incorporate into granules.

The KDs of *Trap1*, *Nipped-A*, *Mcm3*, *tud*, and *Pfas* affected the number and the size of granules (Figures 5Ci and 5Cii). Specifically, KD of *tud* and *Pfas* reduced their number

and the size (Figure 5Ci,ii). Using available fly lines, we demonstrated that OE of *tud* (*tud* OE) increased the size of germ granules and induced their branching (Figures S6Bi–S6Biii), while OE of *Pfas* (*Pfas* OE) reduced germ granules size (Figures S6Ai and S6Aii). Thus, *tud* and *Pfas* control germ granules by regulating their stability and anchoring or by regulating the stability and condensation of Osk protein.

Finally, KDs of *Trap1*, *Nipped-A*, and *Mcm3* reduced the number of granules by 30.5% (*Trap1*) to 37.3% (*Nipped-A*) and increased their size by 29.5% (*Trap1*) to 90.8% (*Mcm3*) (Figures 5Ci and 5Cii). While the fusion of granules could partially explain the increase in germ granule size, enhanced Osk protein expression, enhanced stability, or increased condensation were likely the major driver of germ granule growth.

Germ granule mRNAs encode proteins required for PGC formation and abdominal segmentation.[27] To evaluate whether the 21 hit genes regulated the function of germ granules in addition to their phenotype, we counted the number of PGCs and abdominal segments upon their KD. We observed that KD of *Nipped-A* had no effect, while KDs of *Mcm3*, *Mcm5*, *Pfas*, *eIF2α*, *wisp*, *Sec31*, *aub*, *sub*, *lark*, *Klp3A*, and *Khc* arrested progression through early embryogenesis, which prevented us from studying the effect of these genes on PGC formation and abdominal segmentation (Figures S6C and S6D; Table S1). However, KD of nine genes reduced the number of PGCs and/or abdominal segments (Figures S6C and S6D; Table S1). Of these, *Vas* and *Tud* have been described in this role before,[56–59] while *Pgam5*, *Usp7*, *CG5641*, *CG7878*, *Trap1*, *Hrb98DE*, and *CG2246* have not. Thus, these nine genes regulated not only the phenotype of germ granules but also their function.

Proteins of the ER, NPC, and cytoskeleton regulate the distribution of germ granules

We identified nine genes, *Srp68*, *Sec63*, *CG8507*, *RpL26*, *Elys*, *Nup205*, *Apl*, *RanBPM*, and *Dlic*, as regulators of germ granule distribution (Figure 6A). To our knowledge, these severe distribution phenotypes have not been observed for *Drosophila* germ granules before. The KD of these genes caused branching of germ granules that ranged from mild (e.g., *RanBPM*) to severe (e.g., *Srp68*, *Sec63*, *Elys*, and *Dlic*) (Figures 4B, 6A, and 6B). With the exception of *RpL26* and *Apl*, whose KD efficiencies were 99.7% and 94.1%, respectively, the KD efficiencies for other genes ranged from 60.9% (*Srp68*) to 89.2% (*Sec63*) as measured by qRT-PCR analysis (Table S1). The degree of gene KDs and redundancy in gene function may, in part, account for the range in the phenotypes observed for frequency and the severity of distorted granule distribution.

Previous studies and gene annotations reveal that these genes encode for proteins of the ER (*Srp68*, *Sec63*, *CG8507*, *Rpl26*), NPC (*Elys*, *Nup205*, *Apl*), and cytoskeleton (*RanBPM*, *Dlic*) (Figure 6C). They participate in co-translational and post-translational translocation of proteins into the ER (*Srp68* and *Sec63*, respectively[60]), folding and localization of the low-density lipoprotein (LDL) receptor-related protein (*CG8507*) (predicted; Flybase), form the scaffold of the central NPC channel (*Elys* and *Nup205*),[61] control nuclear import (*Apl*) (predicted; Flybase), organize microtubules (*RanBPM*),[62] and participate in dynein-mediated transport (*Dlic*).[63] In addition, *RpL26* encodes a protein of the 60S large ribosomal subunit that is required for interaction of the ribosome with the Sec61 translocon and for

resolution of stalled ribosomes in the translocon during co-translational translocation.[64,65] Of these, only Srp68 was an RBP (Table S1).

The association of *Drosophila* germ granules with the cytoskeleton is well established (see section ‘‘discussion‘‘). However, their interactions with the ER and NPCs have not been thoroughly investigated. We observed that germ granules readily co-localized with RFP-KDEL (Figures 6Di, 6Dii, and S7A), an ER marker.[66] As the PGCs formed, germ granules remained co-localized with the ER, which also became enriched at the posterior (Figure 6Diii), further supporting our observations that germ granules interacted with the ER. Consistent with this finding, EM of early embryos revealed contacts between germ granules and the ER.[67] In addition, Nup107-GFP, an NPC marker,[68] also co-localized with germ granules (Figures 6E and S7A), demonstrating that germ granules also interacted with NPCs. Importantly, Osk immunoprecipitated other ER, NPC, and cytoskeletal proteins. However, KDs of these genes, although efficient (Table S1), had no phenotype. Since branched granules were also observed in embryos that expressed WT Osk and Vasa (Figures S4C−S4F), we conclude that GFP tagging of these two proteins did not cause branching. Thus, the nine genes that we identified were *bona fide* and specific regulators of germ granule distribution.

To determine whether KDs of these genes affected other aspects of germ granule formation, we quantified the efficiency of accumulation of Osk or Vasa proteins. Due to the branching of granules, we were unable to detect individual granules. Instead, we quantified the total amount of Osk:GFP and Vasa:GFP fluorescence at the posterior. We found that, for most genes, their KDs had no significant effect on the levels of Osk:GFP or Vasa:GFP (Figure 6F). Since Osk:GFP and Vasa:GFP proteins are highly concentrated in germ granules,[26] our data suggest that these gene KDs did not affect the number of granules formed but only altered their spatial arrangement. The exceptions were *Srp68*, *CG8507*, and *Apl*, whose KDs decreased Osk:GFP levels. *Osk* mRNA localized normally upon KD of *CG8507*, suggesting that a reduced accumulation of Osk:GFP in these embryos could have resulted from reduced *osk* translation, reduced Osk protein stability, or inefficient granule formation or anchoring. In contrast, KD of *Apl* and *Srp68* also reduced localization of *osk* mRNA (Figure S7B), which likely decreased Osk protein levels. Expression of *osk* mRNA was unaffected (Figure S7C), indicating that, apart from the distribution of germ granules, *Apl* and *Srp68* also regulated localization of *osk* transcripts to the posterior.

However, KD of *Srp68*, *Sec63*, *CG8507*, *RpL26*, *Elys*, *Nup205*, *Apl*, and *Dlic* did not reduce the number of PGCs and abdominal segments, while KD of RanBPM arrested progression through early embryogenesis (Figures S7D and S7E; Table S1). Thus, these genes primarily regulated the distribution of germ granules.

In summary, we demonstrate that the formation of *Drosophila* germ granules is precisely controlled and primarily driven by proteins, which regulate germ granule number, size, and anchoring to the ER, NPCs, and the cytoskeleton (Figure 7A). Their formation is mechanistically distinct from the RNA-dependent condensation observed for stress granules and P-bodies. However, individual components rely differently on RNA for their enrichment

in germ granules, indicating that multiple intermolecular interactions driven by proteins and RNA control the size and composition of germ granules.

DISCUSSION

Regulation of germ granules by mRNA

We report that, contrary to other RNA granules,[5,8–16] the nucleation and persistence of the *Drosophila* germ granules is independent of Osk-bound mRNAs. An important implication of this finding is that the function of a particular RNA granule could dictate the role that RNA plays in its formation. In granules that mostly store post-transcriptionally inactive RNAs, such as stress granules and P-bodies, RNA could be required for the formation and persistence of granules. However, in granules that contain translationally active mRNAs, such as the *Drosophila* germ granules, RNA may serve primarily as a substrate for post-transcriptional regulation rather than provide a scaffold for their formation.

However, we also observed that RNase A treatment reduced accumulation of a core germ granule protein, Aubergine (Figures S3E and S3F), indicating that RNA is important for the compositional specificity of germ granules. In addition, the removal of RNA increased the size of germ granules (Figure 3D), indicating that RNA limits condensation of Osk protein and germ granule growth, as observed in other RNA granules.[16,69] In support of this observation, when Short Oskar lacking its RNA-binding domain is expressed in S2 cells, it forms granules that are much bigger than those formed by WT Short Oskar.[26] We further observed that, as the amount of Oskar increased during oogenesis, new germ granules formed rather than increased in their size, which also rapidly enriched mRNAs. Together, our data raise the possibility that mRNAs could indirectly promote their own enrichment at the posterior. By limiting Osk condensation, mRNAs could stimulate the formation of new germ granules and thus promote their own enrichment at the posterior.

Regulators of germ granule number and size

While the protein-driven condensation of *Drosophila* germ granules is distinct from the RNA-dependent formation observed for stress granules and P-bodies, our study also revealed similarities in how these distinct granule form. Like stress granules and P-bodies,[5–7,70] we observed that germ granules rely on RBPs, protein chaperones, and degradation factors for condensation. Notably, these regulators often require energy for their ability to control condensation.[7,19] In agreement with these findings, we identified CG2246 and *Pfas* proteins, which are involved in the biosynthesis of purine nucleotides (FlyBase) as germ granule regulators. These two proteins could supply energy to helicases, chaperones, and translation machinery to control *osk* mRNA localization and translation as well as Osk condensation. Finally, we identified Mcm3 and Mcm5 proteins, subunits of the Mcm2–7 DNA replication complex,[71] as germ granule regulators (Figures 5Ci, 5Cii, and S5). Importantly, *Mcm4*, another subunit of the Mcm2–7 complex,[71] and *pontin* (human RUVBL1), a AAA+ DNA helicase involved in DNA repair,[72] also co-purified with Short Oskar,[51] but, unlike Mcm3 and Mcm5, had no effect on germ granule formation despite efficient KDs (Table S1). Interestingly, all four proteins also regulate mammalian stress

granules[7]; however, our data indicate that only *Mcm3* and *Mcm5* function in both RNA granules.

Regulation of germ granule distribution by the ER, NPC, and cytoskeleton

We observed that *Drosophila* germ granules associated with ER, NPC, and cytoskeleton, a feature that is shared by many RNA granules, including stress granules, P-bodies, TIS granules, Whi3 granules, P granules, and the perinuclear nuage.[73–79]

The link between the cytoskeleton and germ granules is well established. F actin anchors germ granules in oocytes and early embryos prior to the formation of PGCs and Osk is required for this process, while astral microtubules and dynein motors organize germ granules into crescents that abut the nuclei of PGCs.[48] Upon localization, *osk* mRNA translates into two isoforms, Long Oskar and Short Oskar, that differ in the first 138 amino acids.[80] Short Oskar forms germ granules,[49,80] while Long Oskar stimulates the formation of F actin and thereby anchoring of germ granules.[36–38,80] However, an additional, actin-independent mechanism immobilizes germ granules at the posterior,[35] possibly involving the ER and NPC proteins we uncovered in this study.

Interestingly, the endocytic pathway is also required for *osk* mRNA localization and the formation of germ granules in the fly.[37,41,81,82] Indeed, Long Oskar almost exclusively associates with the endocytic membranes at posterior cortex,[41] where it stimulates endocytosis to entrap and maintain *osk* mRNA and germ granules at the posterior.[35,37,41,82] However, while the primary function of Long Oskar is to enhance endocytosis and the formation of F actin protrusions, the maintenance of WT levels of germ granules at the posterior requires activity of both Osk isoforms.[41] These observations suggest that Short Oskar itself, or the genes products enriched in germ granules, stimulates endocytosis and rearranges the actin cytoskeleton and that the association of germ granules with the ER could facilitate this process.

A branched germ granule phenotype suggested that anchors that immobilized granules at the posterior lost their spatial organization and coalesced. Alternatively, this phenotype could have been caused by a change in their biophysical properties, such that granules can interact with each other but could not completely fuse. In addition, ER and the NPCs could also promote granule condensation. In *A. gossypii*, the recruitment of Whi3 to the ER membranes initially promotes condensation of Whi3 and afterward prevents it, which limits the growth of Whi3 granules.[75] Interestingly, we observed that the condensation of Osk protein and therefore the size of germ granules is controlled, perhaps through its interactions with the ER or the NPC. Branching of germ granules further indicates that, upon contact, germ granules did not fuse, a behavior suggestive of a change in the material properties and hardening of granules.[16] Thus, similar to Whi3, the membrane of the ER and the nuclear envelope could regulate the number and size of germ granules by regulating condensation of Osk protein.

The role of ER and NPCs in germ granule function

Germ cells are immortal cells required for the continuity of the species. They achieve this feat by extensive transcriptional and post-transcriptional regulation coupled with

communication between germ cells and surrounding somatic cells, which enables germ cells to establish, promote, and protect their totipotent potential.

Association of germ granules with the ER and NPCs carries important functional consequences for the development of germ cells. Up to 200 different mRNAs enrich in germ granules[83] and only four (*nos*, *pgc*, *gcl*, and *CycB*) have been extensively characterized for their role in germline development.[27] Some germ granule mRNAs might code for signaling and receptor proteins required for cell-to-cell communication during germline development and could translate on the ER to deliver regulators to the surface of germ cells (Figure 7B). In addition, the genetic material of PGCs is extensively regulated to prevent somatic differentiation and preserve totipotency of PGCs.[84] For instance, the Pgc protein coded by the germ granule *pgc* mRNA inhibits recruitment of the transcription elongation factor P-TEFb to transcription sites and prevents differentiation of PGCs to somatic cells.[85] Here, the association of germ granules with the NPCs (Figure 7B) could augment nuclear import of regulators such as Pgc to bolster the efficiency of gene expression regulation in PGCs. Thus, association of germ granules with the ER and NPCs could play a central role not only in the formation of the *Drosophila* germ granules but also in linking the germ granules, ER, and NPCs with the establishment of the germ cell lineage.

Limitations of the study

Studies of stress granules revealed that RNA promotes their formation in two ways. First, RNA binding triggers conformational changes of stress granule nucleator proteins, thereby promoting their condensation.[5] Second, RNA enables protein:RNA and RNA:RNA interactions and provides a scaffold for protein condensation.[17,18] In contrast to these findings, we observed that mutant Osk lacking its RNA-binding domain nevertheless condenses and forms granules. However, since only Osk-bound mRNAs were investigated, it is possible that other mRNAs could trigger Osk condensation indirectly, perhaps by promoting protein-protein interactions between Osk and its binding partners that themselves interact with these mRNAs. Furthermore, since the 30 hit genes are essential, the reduction in PGC numbers and abdominal segments upon their knockdown could have resulted from the lack of these essential activities rather than misregulation of germ granule function, per se.

STAR★METHODS

RESOURCE AVAILABILITY

Lead contact—Further information and requests for resources and reagents should be directed to and will be fulfilled by the lead contact, Tatjana Trcek (ttrcekp1@jhu.edu).

Materials availability—Publicly available reagents used in this study and unique reagents generated in this study are available from the lead contact upon request.

Data and code availability

- Microscopy data generated in this study will be shared by the lead contact upon request.

- This paper does not report original code.
- Any additional information required to reanalyze the data reported in this paper is available from lead contact upon request.

EXPERIMENTAL MODEL AND STUDY PARTICIPANT DETAILS

Fly lines—All *Drosophila melanogaster* lines used in this study were raised on standard cornmeal agar medium at 60% humidity, 25°C, 12h light/12h dark cycle. In all experiments, 3 to 7 days old females were used. To count germ granules, females expressing Osk:EGFP (*w;; osk::EGFP^{KI}*; Gift from Graydon Gonsalvez lab) or Vasa:EGFP (*w; vas::EGFP^{KI}*; Gift from Akira Nakamura lab[86]) tagged with the CRISPR/Cas9 genome editing were used. Vasa: GFP transgenes (*y,w; P[E GFP-vas w+]cyIII*),[44] Tud:EGFP (*w: HA_EGFP:: tud^{KI}*),[86] Aub:EGFP (*w: EGFP::aub^{KI}/cyo*),[86] VasamCherry (*w:vas::mCherry^{KI}*)[86],*mnk aub^{HN2}* (*mnk aub^{HN2}/cyo*),[87] *mnk, aub^{QC42}* (*mnk, aub^{QC42}/cyo*),[87] *tud^{C30-51}* (*Tud^{C30-51}/cyo*),[88] *tud1* (*tud1/cyo*),[88] *vas^{D1}* (*yw;vas$^{D1\ b\ cn}$/cyo*)[89] and *vas1* (*vas1/cyo*)[89] flies were described before. The full list of flies and their genotypes is provided in Table S2.

METHOD DETAILS

Microscopy and deconvolution—Images were acquired with a vt-instant Structured Illumination Microscope (vt-iSIM; BioVision Technologies) equipped with the 405nm 100mw, 488nm 150Mw, 561nm 150mW, 642nm 100mW and 445nm 75 mW lasers, two ORCA-Fusion sCMOS cameras and the Leica HC PL APO 63x/1.30 GLYC CORR CS2, HC PL APO 63x/1.40 OIL CS2 and HC PL APO 100x/1.47 OIL CORR TIRF objectives. Images were acquired in three dimensions (3D) and afterward deconvolved using Huygens (Scientific Volume Imaging), as described before.[90]

Embryo collection—Embryos were collected as described before.[90] In short, flies were placed in an egg collection cage and mounted with an apple juice plate containing a dollop of yeast paste. The cage was placed into a 25°C incubator and females were allowed to lay eggs, after which the embryos were dechorionated with the bleach solution, collected into the egg collection basket and washed to remove bleach. Eggs were then fixed in a solution containing saturated heptane and paraformaldehyde fixative at R/T for 20 min. Afterward, the embryos were devitellinized by methanol cracking, washed with 100% methanol and store in 100% methanol at 4°C until further use.

Oocyte dissection and fixation—Three to seven-day old, well-fed females were anesthetized and dissected in a chilled 1x PBS buffer. Individual oocytes were separated from ovarioles into stages 10A, 10B, 11 and 12 and stages 13 and 14. They were then fixed for 20 min in 4% paraformaldehyde (Electron Microscopy Sciences; # 15713) at room temperature (RT), followed by three washes in 1XPBS.[90] Oocytes were then washed 3 times with methanol and stored at 4°C until use.

smFISH in embryos and oocytes—smFISH procedure and probes used to label mRNAs were described before.[44,90]

Timing of oocyte stages and embryonic nuclear cycles—Staging of oocytes and embryonic nuclear cycles was done as described previously.[94,95] In short, oocytes and embryos were stained with the DAPI nuclear stain to determine the position and the number of the nuclei in oocytes and embryos, which then enabled us to stage the oocytes and embryos into the correct oogenic stage and nuclear cycle.

Egg hatching—To quantify the egg hatching rate of the Osk:GFP CRISPR/Cas line, 20 to 40 virgin females were collected and mated with WT (W^{1118}) males. 4 days later, they were caged and allowed to lay eggs overnight at 25°C on apple juice plates supplemented with yeast paste,[90] after which the number of laid eggs was determined. The plates were incubated for two more days at 25°C after which the number of hatched eggs was determined. To quantify the egg hatching rate of individual RNAi lines, 5–10-day old females mated with the males derived from the same cross. Afterward, the egg hatching rate was scored as indicated above.

***In vivo* RNase assay—**Three to seven-day old, well-fed females were anesthetized and dissected in Schneider's *Drosophila* Medium (Thermo Fisher Scientific; #21720024) supplemented with FBS (10%; Invitrogen; #10082–139), penicillin-streptomycin (1%; Fisher; #15140122), and insulin (200 μg/mL; Sigma-Aldrich; #I5500–500MG) prewarmed to 25°C, which enabled a prolonged investigation of germ granules in live oocytes.[96] Individual oocytes were removed from ovarioles with care. The oocytes were separated into stages 10 through 12 and stages 13 and 14. The oocytes were then washed with 1x PBTx (1XPBS that contains 1% Triton X-100) and incubated at RT for 15 min. Dissection time between the removal of the first pair of ovaries and the incubation in PBTx was kept to no more than 30 min. The PBTx was removed and the oocytes were washed once with supplemented Schneider's medium. The oocytes were then treated with supplemented Schneider's medium alone or supplemented Schneider's medium containing insulin and RNase A (100 mg/mL; Millipore Sigma; # 10109169001), both prewarmed to 25°C. The oocytes were then incubated at 25°C for 30 min and afterward fixed as described above or homogenized in Trizol reagent (Thermo Fisher Scientific; # 15596026) for RNA isolation (see below).

***In vitro* RNase assay—**This assay was modified from.[26,97] Embryos were collected as described above. After dechorionation, embryos were added to a 1.7 mL tube containing 1xPBS by carefully removing them from the mesh with a paintbrush. The PBS was removed and replaced with cold lysis buffer containing 50 mM Tris at pH 7.6, 50 mM NaCl, 5 mM MgCl2, 1 mM β-mercaptoethanol (Millipore Sigma; # 444203–250ML), 1× protease inhibitor complete mini EDTA free (Sigma, #11836170001) and initially supplemented with 0.4 U/μL RNase Out (Invitrogen; # 10777019). All subsequent steps were performed at 4°C. The embryos were then homogenized and centrifuged at 2000g for 2 min. The supernatant was removed and split into two equal fractions. Both fractions were centrifuged at RT at 10,000g for 10 min. The supernatant was removed and the pellet was either resuspended with cold lysis buffer (50 mM Tris at pH 7.6, 50 mM NaCl, 5 mM MgCl2, 1 mM β-mercaptoethanol, 1× protease inhibitor) containing 1ug/uL RNase A or with cold lysis buffer (50 mM Tris at pH 7.6, 50 mM NaCl, 5 mM MgCl2, 1 mM β-mercaptoethanol, 1×

protease inhibitor) supplemented with 0.4 U/μl RNase Out inhibitor. The resuspended pellets were then added to a Lab-Tek II 8 Chambered Coverglass dish (Thermo Fisher Scientific; # 155409PK) and incubated for 1 h at RT. The samples were then imaged. After imaging the resuspensions were added to a 1.7 mL tube with 100uL Trizol for subsequent RNA isolation (see below).

RNA isolation—Total RNA from RNase experiments was isolated from Trizol reagent using Zymogen Direct-zol Microprep RNA Kit and treated on column with DNase I (Zymo Research, R2061).

Denaturing RNA gel—After RNA extraction wit Zymo Direct-zol Kit, samples were loaded onto a 0.5X TAE gel (1.5% agarose) using 2X RNA Loading Dye (NEB, N0362) and examined after running the gel for 80 min at 70 V.

QUANTIFICATION AND STATISTICAL ANALYSIS

Statistical analysis—A two-tailed t test was used to calculate statistical significance using SigmaPlot. Statistical details of experiments including sample size, error type and number of biological and technical replicates can be found in figure legends.

qRT-PCR—Quantitative PCR analyses was performed as described before[43] using a CFX Opus 96 Real-Time PCR System from Bio Rad. The qRT-PCR primers used in this study are listed in Table S3. Per condition, three biological replicates and three technical replicates were analyzed. Flies expressing a Vasa:GFP transgene were used for normalization.

Quantifying the number and size of germ granules—The number and size of germ granules was determined using a spot detection algorithm called Airlocalize.[90,91] The embryos were imaged in 3D with an HC PL APO 100x/1.47 OIL CORR TIRF objective after which the images were deconvolved.[90] To measure germ granule size, we quantified the total fluorescent intensity of Osk:GFP or Vasa:GFP per granule, which reflected the amount of Oskar and Vasa proteins per granule and thus served as a proxy for the size of germ granules. Airlocalize detects individual, fluorescently labeled spots such as germ granules using a 3D Gassian kernel to find the center and intensity of each spot within a 3D image. Subtraction of the local background during spot detection increased the robustness of spot identification and localization against a high autofluorescent background.[90] The number and sizes of germ granules for embryos laid by WT and mutant flies are listed in Table S1.

Quantifying the change in the number and size of germ granules upon KD with RNAi—The number and size of germ granules upon KD all 37 genes are reported in the Table S1. Only genes that trigger changes in the number or size of germ granules greater than 30% were considered as inducing significant differences. The bars in Figures 5 and S5 show a percent change in the number or size of germ granules labeled with Osk:GFP (*vas*, *CG5641*, *Trap1*, *tud*) and Vasa:GFP (*CG7878*,*Usp7*, *eIF2α*, *Pgam5*, *Nipped-A*, *Mcm3*, *Pfas*) upon KD of a particular gene. The percent change was calculated relative the number and size of germ granules in WT embryos expressing only Osk:GFP or Vasa:GFP. Labeling of germ granules with Osk:GFP or Vasa:GFP depended on the chromosomal integration of the

RNAi construct (Table S2). *tud*$^{C30-51}$, *tud,1 vas*^{D1} and *vas*^{PD} mutant alleles were used to quantify changes in the number and size of germ granules in the absence of Tudor and Vasa proteins. Mean number 4 to 59 embryos per genotype were quantified and afterward the percent change calculated.

Quantifying the span of germ granules—Embryos and oocytes were imaged in 3D using a 400nm Z step. Afterward, the Z plane in which the germ granule produced the longest span was analyzed using a line segmentation tool in ImageJ[92] (Figure S1D). Segmented lines were drawn to trace the periphery of the oocyte in the chosen Z plane, tracing where germ granules were present. The total distance of the drawn lines was then measured using the Measure feature in ImageJ.

Quantifying the distribution of germ granules—In describing changes in the spatial organization of germ granules, we employed the term ‘‘distribution’’, as this term describes the spread of objects over an area without implying that that the number of these objects has also changed among experiments. In WT embryos, where individual germ granules appeared as well separated, individual spots, we quantified the distribution of germ granules by measuring the number of granules per square micrometer of germ plasm. However, in mutant embryos, where germ granules no longer presented as individual entities, we only qualitatively noted a change in their spatial distribution. We avoided the term ‘‘morphology’’, since the size of individual germ granules is within the resolution limit of SIM,[46,47] which prevented us to unequivocally determine whether the KDs of genes we studied affected the appearance of individual germ granules or not. We also avoided the term ‘‘density’’, since upon knockdown of genes we were unable to reliably detect and quantify individual germ granules and report changes in their number. To calculate the germ granule distribution, a two-dimensional (2D) region of interest (ROI) of known micrometer dimensions was cropped from the center of an image of the germ plasm and the number of granule determined as described above and before.[90] The 2D regions were averaged across several Z slices, as different regions of the germ plasm were in focus across the z stack.

Quantifying total fluorescence intensity—Total fluorescence of Oskar:GFP, Vasa:GFP and of smFISH-stained mRNA at the posterior pole was measured in ImageJ Fiji using 3D Objects Counter as described before.[44]

Immunofluorescence and PGC counting—Three hours after egg laying, dechorionated embryos were fixed and immunostained using polyclonal rabbit antisera at 1:1000 dilution. Embryos were then imaged in 3D and PGCs counted in a 3D stack, as previously described.[26]

Evaluating segmentation defects by detecting *ftz* gene expression—Three to 4 h after egg laying, dechorionated embryos were fixed and stained with smFISH probes (Table S4). The number of abdominal segments labeled with the *ftz* stain counted, as described previously.[98] In short, WT embryos develop seven *ftz* stripes while mutations that affect abdomen formation will develop fewer segments. These can be counted using low magnification objective lens.

Co-localization measurements—Colocalization measurements between germ granules and the ER or NPCs were measured in ImageJ Fiji using PCC(Costes) analysis function of the JaCoP plugin[93] as described before.[44]

Supplementary Material

Refer to Web version on PubMed Central for supplementary material.

ACKNOWLEDGMENTS

We thank Drs. Gonsalves, Lehmann, Nakamura, and Theurkauf for sharing flies with us, and Drs. Mainak Bose, Xin Chen, Anne Ephrussi, John Kim, and Trcek lab members for critical reading of the manuscript. This research was supported by the NICHD R00HD088675 and the NIGMS R35GM142737 grants awarded to T.T.

REFERENCES

1. Shukla S, and Parker R (2016). Hypo- and Hyper-Assembly Diseases of RNA-Protein Complexes. Trends Mol. Med 22, 615–628. 10.1016/j.molmed.2016.05.005. [PubMed: 27263464]
2. Tian S, Curnutte HA, and Trcek T (2020). RNA Granules: A View from the RNA Perspective. Molecules 25, 3130. 10.3390/molecules25143130. [PubMed: 32650583]
3. Hyman AA, Weber CA, and Jülicher F (2014). Liquid-liquid phase separation in biology. Annu. Rev. Cell Dev. Biol 30, 39–58. 10.1146/annurev-cellbio-100913-013325. [PubMed: 25288112]
4. Gomes E, and Shorter J (2019). The molecular language of membraneless organelles. J. Biol. Chem 294, 7115–7127. 10.1074/jbc.TM118.001192. [PubMed: 30045872]
5. Yang P, Mathieu C, Kolaitis RM, Zhang P, Messing J, Yurtsever U, Yang Z, Wu J, Li Y, Pan Q, et al. (2020). G3BP1 Is a Tunable Switch that Triggers Phase Separation to Assemble Stress Granules. Cell 181, 325–345.e28. 10.1016/j.cell.2020.03.046. [PubMed: 32302571]
6. Owen I, and Shewmaker F (2019). The Role of Post-Translational Modifications in the Phase Transitions of Intrinsically Disordered Proteins. Int. J. Mol. Sci 20, 5501. 10.3390/ijms20215501. [PubMed: 31694155]
7. Jain S, Wheeler JR, Walters RW, Agrawal A, Barsic A, and Parker R (2016). ATPase-Modulated Stress Granules Contain a Diverse Proteome and Substructure. Cell 164, 487–498. 10.1016/j.cell.2015.12.038. [PubMed: 26777405]
8. Ma WR, Zheng G, Xie W, and Mayr C (2021). In Vivo Reconstitution Finds Multivalent RNA-RNA Interactions as Drivers of Meshlike Condensates. Elife 10, e64252, ARTN. 10.7554/eLife.64252. [PubMed: 33650968]
9. Cougot N, Babajko S, and Séraphin B (2004). Cytoplasmic foci are sites of mRNA decay in human cells. J. Cell Biol 165, 31–40. 10.1083/jcb.200309008. [PubMed: 15067023]
10. Decker CJ, Burke JM, Mulvaney PK, and Parker R (2022). RNA is required for the integrity of multiple nuclear and cytoplasmic membraneless RNP granules. EMBO J 41, e110137. 10.15252/embj.2021110137. [PubMed: 35355287]
11. Fernandes N, and Buchan JR (2020). RPS28B mRNA acts as a scaffold promoting cis-translational interaction of proteins driving P-body assembly. Nucleic Acids Res 48, 6265–6279. 10.1093/nar/gkaa352. [PubMed: 32396167]
12. Fuller GG, Han T, Freeberg MA, Moresco JJ, Ghanbari Niaki A, Roach NP, Yates JR 3rd, Myong S, and Kim JK (2020). RNA promotes phase separation of glycolysis enzymes into yeast G bodies in hypoxia. Elife 9, e48480. 10.7554/eLife.48480. [PubMed: 32298230]
13. Langdon EM, Qiu Y, Ghanbari Niaki A, McLaughlin GA, Weidmann CA, Gerbich TM, Smith JA, Crutchley JM, Termini CM, Weeks KM, et al. (2018). mRNA structure determines specificity of a polyQ-driven phase separation. Science 360, 922–927. 10.1126/science.aar7432. [PubMed: 29650703]

14. Lee CYS, Putnam A, Lu T, He S, Ouyang JPT, and Seydoux G (2020). Recruitment of mRNAs to P granules by condensation with intrinsically-disordered proteins. Elife 9, e52896. 10.7554/eLife.52896. [PubMed: 31975687]
15. Smith J, Calidas D, Schmidt H, Lu T, Rasoloson D, and Seydoux G (2016). Spatial Patterning of P Granules by RNA-Induced Phase Separation of the Intrinsically-Disordered Protein MEG-3. Elife 5. 10.7554/eLife.21337.
16. Zhang H, Elbaum-Garfinkle S, Langdon EM, Taylor N, Occhipinti P, Bridges AA, Brangwynne CP, and Gladfelter AS (2015). RNA Controls PolyQ Protein Phase Transitions. Mol. Cell 60, 220–230. 10.1016/j.molcel.2015.09.017. [PubMed: 26474065]
17. Van Treeck B, and Parker R (2018). Emerging Roles for Intermolecular RNA-RNA Interactions in RNP Assemblies. Cell 174, 791–802. 10.1016/j.cell.2018.07.023. [PubMed: 30096311]
18. Van Treeck B, Protter DSW, Matheny T, Khong A, Link CD, and Parker R (2018). RNA self-assembly contributes to stress granule formation and defining the stress granule transcriptome. Proc. Natl. Acad. Sci. USA 115, 2734–2739. 10.1073/pnas.1800038115. [PubMed: 29483269]
19. Hondele M, Sachdev R, Heinrich S, Wang J, Vallotton P, Fontoura BMA, and Weis K (2019). DEAD-box ATPases are global regulators of phase-separated organelles. Nature 573, 144–148. 10.1038/s41586-019-1502-y. [PubMed: 31435012]
20. Tauber D, Tauber G, Khong A, Van Treeck B, Pelletier J, and Parker R (2020). Modulation of RNA Condensation by the DEAD-Box Protein eIF4A. Cell 180, 411–426.e16. 10.1016/j.cell.2019.12.031. [PubMed: 31928844]
21. Ephrussi A, and Lehmann R (1992). Induction of Germ-Cell Formation by Oskar. Nature 358, 387–392. 10.1038/358387a0. [PubMed: 1641021]
22. Illmensee K, and Mahowald AP (1974). Transplantation of Posterior Polar Plasm in Drosophila - Induction of Germ-Cells at Anterior Pole of Egg. P Natl Acad Sci USA 71, 1016–1020. 10.1073/pnas.71.4.1016.
23. Illmensee K, Mahowald AP, and Loomis MR (1976). The ontogeny of germ plasm during oogenesis in Drosophila. Dev. Biol 49, 40–65. 10.1016/0012-1606(76)90257-8. [PubMed: 815119]
24. Jazdowska-Zagrodzińska B (1966). Experimental studies on the role of ‘polar granules’ in the segregation of pole cells in Drosophila melanogaster. J. Embryol. Exp. Morphol 16, 391–399. [PubMed: 6006943]
25. Lehmann R, and Nüsslein-Volhard C (1986). Abdominal segmentation, pole cell formation, and embryonic polarity require the localized activity of oskar, a maternal gene in Drosophila. Cell 47, 141–152. 10.1016/0092-8674(86)90375-2. [PubMed: 3093084]
26. Kistler KE, Trcek T, Hurd TR, Chen R, Liang FX, Sall J, Kato M, and Lehmann R (2018). Phase transitioned nuclear Oskar promotes cell division of Drosophila primordial germ cells. Elife 7, e37949. 10.7554/eLife.37949. [PubMed: 30260314]
27. Trcek T, and Lehmann R (2019). Germ granules in Drosophila. Traffic 20, 650–660. 10.1111/tra.12674. [PubMed: 31218815]
28. Markussen FH, Michon AM, Breitwieser W, and Ephrussi A (1995). Translational Control of Oskar Generates Short Osk, the Isoform That Induces Pole Plasm Assembly. Development 121, 3723–3732. [PubMed: 8582284]
29. Hachet O, and Ephrussi A (2004). Splicing of oskar RNA in the nucleus is coupled to its cytoplasmic localization. Nature 428, 959–963. 10.1038/nature02521. [PubMed: 15118729]
30. Ghosh S, Marchand V, Gáspár I, and Ephrussi A (2012). Control of RNP motility and localization by a splicing-dependent structure in oskar mRNA. Nat. Struct. Mol. Biol 19, 441–449. 10.1038/nsmb.2257. [PubMed: 22426546]
31. Castagnetti S, Hentze MW, Ephrussi A, and Gebauer F (2000). Control of oskar mRNA translation by Bruno in a novel cell-free system from Drosophila ovaries. Development 127, 1063–1068. [PubMed: 10662645]
32. Chekulaeva M, Hentze MW, and Ephrussi A (2006). Bruno acts as a dual repressor of oskar translation, promoting mRNA oligomerization and formation of silencing particles. Cell 124, 521–533. 10.1016/j.cell.2006.01.031. [PubMed: 16469699]

33. Yang N, Yu Z, Hu M, Wang M, Lehmann R, and Xu RM (2015). Structure of Drosophila Oskar reveals a novel RNA binding protein. Proc. Natl. Acad. Sci. USA 112, 11541–11546. 10.1073/pnas.1515568112. [PubMed: 26324911]
34. Jeske M, Bordi M, Glatt S, Müller S, Rybin V, Muller CW, and Ephrussi A (2015). The Crystal Structure of the Drosophila Germline Inducer Oskar Identifies Two Domains with Distinct Vasa Helicase- and RNA-Binding Activities. Cell Rep 12, 587–598. 10.1016/j.cel-rep.2015.06.055. [PubMed: 26190108]
35. Babu K, Cai Y, Bahri S, Yang X, and Chia W (2004). Roles of Bifocal, Homer, and F-actin in anchoring Oskar to the posterior cortex of Drosophila oocytes. Genes Dev 18, 138–143. 10.1101/gad.282604. [PubMed: 14752008]
36. Rongo C, Broihier HT, Moore L, Van Doren M, Forbes A, and Lehmann R (1997). Germ plasm assembly and germ cell migration in Drosophila. Cold Spring Harb. Symp. Quant. Biol 62, 1–11. [PubMed: 9598330]
37. Tanaka T, Kato Y, Matsuda K, Hanyu-Nakamura K, and Nakamura A (2011). Drosophila Mon2 couples Oskar-induced endocytosis with actin remodeling for cortical anchorage of the germ plasm. Development 138, 2523–2532. 10.1242/dev.062208. [PubMed: 21610029]
38. Vanzo NF, and Ephrussi A (2002). Oskar anchoring restricts pole plasm formation to the posterior of the Drosophila oocyte. Development 129, 3705–3714. 10.1242/dev.129.15.3705. [PubMed: 12117819]
39. Spradling A (1993). Developmental Genetics of Oogenesis in the Development of Drosophila melanogaster (CSHL Press), pp. 1–70.
40. Su TT, Campbell SD, and O'Farrell PH (1998). The cell cycle program in germ cells of the Drosophila embryo. Dev. Biol 196, 160–170. 10.1006/dbio.1998.8855. [PubMed: 9576829]
41. Vanzo N, Oprins A, Xanthakis D, Ephrussi A, and Rabouille C (2007). Stimulation of endocytosis and actin dynamics by Oskar polarizes the Drosophila oocyte. Dev. Cell 12, 543–555. 10.1016/j.devcel.2007.03.002. [PubMed: 17419993]
42. Little SC, Sinsimer KS, Lee JJ, Wieschaus EF, and Gavis ER (2015). Independent and coordinate trafficking of single Drosophila germ plasm mRNAs. Nat. Cell Biol 17, 558–568. 10.1038/ncb3143. [PubMed: 25848747]
43. Trcek T, Douglas TE, Grosch M, Yin Y, Eagle WVI, Gavis ER, Shroff H, Rothenberg E, and Lehmann R (2020). Sequence-Independent Self-Assembly of Germ Granule mRNAs into Homotypic Clusters. Mol. Cell 78, 941–950.e12. 10.1016/j.molcel.2020.05.008. [PubMed: 32464092]
44. Trcek T, Grosch M, York A, Shroff H, Lionnet T, and Lehmann R (2015). Drosophila germ granules are structured and contain homotypic mRNA clusters. Nat. Commun 6, 7962. 10.1038/ncomms8962. [PubMed: 26242323]
45. Sinsimer KS, Lee JJ, Thiberge SY, and Gavis ER (2013). Germ plasm anchoring is a dynamic state that requires persistent trafficking. Cell Rep 5, 1169–1177. 10.1016/j.celrep.2013.10.045. [PubMed: 24290763]
46. Mahowald AP (1962). Fine Structure of Pole Cells and Polar Granules in Drosophila Melanogaster. J. Exp. Zool 151, 201–215. 10.1002/jez.1401510302.
47. York AG, Chandris P, Nogare DD, Head J, Wawrzusin P, Fischer RS, Chitnis A, and Shroff H (2013). Instant super-resolution imaging in live cells and embryos via analog image processing. Nat. Methods 10, 1122–1126. 10.1038/nmeth.2687. [PubMed: 24097271]
48. Lerit DA, and Gavis ER (2011). Transport of germ plasm on astral microtubules directs germ cell development in Drosophila. Curr. Biol 21, 439–448. 10.1016/j.cub.2011.01.073. [PubMed: 21376599]
49. Breitwieser W, Markussen FH, Horstmann H, and Ephrussi A (1996). Oskar protein interaction with Vasa represents an essential step in polar granule assembly. Genes Dev 10, 2179–2188. 10.1101/gad.10.17.2179. [PubMed: 8804312]
50. Jeske M, Müller CW, and Ephrussi A (2017). The LOTUS domain is a conserved DEAD-box RNA helicase regulator essential for the recruitment of Vasa to the germ plasm and nuage. Genes Dev 31, 939–952. 10.1101/gad.297051.117. [PubMed: 28536148]

51. Hurd TR, Herrmann B, Sauerwald J, Sanny J, Grosch M, and Lehmann R (2016). Long Oskar Controls Mitochondrial Inheritance in Drosophila melanogaster. Dev. Cell 39, 560–571. 10.1016/j.devcel.2016.11.004. [PubMed: 27923120]
52. Pae J, Cinalli RM, Marzio A, Pagano M, and Lehmann R (2017). GCL and CUL3 Control the Switch between Cell Lineages by Mediating Localized Degradation of an RTK. Dev. Cell 42, 130–142.e7. 10.1016/j.devcel.2017.06.022. [PubMed: 28743001]
53. St Johnston D, Beuchle D, and Nüsslein-Volhard C (1991). Staufen, a gene required to localize maternal RNAs in the Drosophila egg. Cell 66, 51–63. [PubMed: 1712672]
54. Anne J, and Mechler BM (2005). Valois, a component of the nuage and pole plasm, is involved in assembly of these structures, and binds to Tudor and the methyltransferase Capsuleen. Development 132, 2167–2177. 10.1242/dev.01809. [PubMed: 15800004]
55. Anne J, Ollo R, Ephrussi A, and Mechler BM (2007). Arginine methyltransferase Capsuleen is essential for methylation of spliceosomal Sm proteins and germ cell formation in Drosophila. Development 134, 137–146. 10.1242/dev.02687. [PubMed: 17164419]
56. Thomson T, and Lasko P (2004). Drosophila tudor is essential for polar granule assembly and pole cell specification, but not for posterior patterning. Genesis 40, 164–170. 10.1002/gene.20079. [PubMed: 15495201]
57. Boswell RE, and Mahowald AP (1985). tudor, a gene required for assembly of the germ plasm in Drosophila melanogaster. Cell 43, 97–104. [PubMed: 3935320]
58. Schüpbach T, and Wieschaus E (1986). Maternal-effect mutations altering the anterior-posterior pattern of the Drosophila embryo. Rouxs Arch. Dev. Biol 195, 302–317. 10.1007/BF00376063.
59. Durdevic Z, and Ephrussi A (2019). Germ Cell Lineage Homeostasis in Drosophila Requires the Vasa RNA Helicase. Genetics 213, 911–922. 10.1534/genetics.119.302558. [PubMed: 31484689]
60. Jung SJ, and Kim H (2021). Emerging View on the Molecular Functions of Sec62 and Sec63 in Protein Translocation. Int. J. Mol. Sci 22, 12757. 10.3390/ijms222312757. [PubMed: 34884562]
61. Raices M, and D'Angelo MA (2012). Nuclear pore complex composition: a new regulator of tissue-specific and developmental functions. Nat. Rev. Mol. Cell Biol 13, 687–699. 10.1038/nrm3461. [PubMed: 23090414]
62. Suresh B, Ramakrishna S, and Baek KH (2012). Diverse roles of the scaffolding protein RanBPM. Drug Discov. Today 17, 379–387. 10.1016/j.drudis.2011.10.030. [PubMed: 22094242]
63. Amrute-Nayak M, and Bullock SL (2012). Single-molecule assays reveal that RNA localization signals regulate dynein-dynactin copy number on individual transcript cargoes. Nat. Cell Biol 14, 416–423. 10.1038/ncb2446. [PubMed: 22366687]
64. Walczak CP, Leto DE, Zhang L, Riepe C, Muller RY, DaRosa PA, Ingolia NT, Elias JE, and Kopito RR (2019). Ribosomal protein RPL26 is the principal target of UFMylation. Proc. Natl. Acad. Sci. USA 116, 1299–1308. 10.1073/pnas.1816202116. [PubMed: 30626644]
65. Wang L, Xu Y, Rogers H, Saidi L, Noguchi CT, Li H, Yewdell JW, Guydosh NR, and Ye Y (2020). UFMylation of RPL26 links translocation-associated quality control to endoplasmic reticulum protein homeostasis. Cell Res 30, 5–20. 10.1038/s41422-019-0236-6. [PubMed: 31595041]
66. Frescas D, Mavrakis M, Lorenz H, Delotto R, and Lippincott-Schwartz J (2006). The secretory membrane system in the Drosophila syncytial blastoderm embryo exists as functionally compartmentalized units around individual nuclei. J. Cell Biol 173, 219–230. 10.1083/jcb.200601156. [PubMed: 16636144]
67. Thomson T, Liu N, Arkov A, Lehmann R, and Lasko P (2008). Isolation of new polar granule components in Drosophila reveals P body and ER associated proteins. Mech. Dev 125, 865–873. 10.1016/j.mod.2008.06.005. [PubMed: 18590813]
68. Hampoelz B, Schwarz A, Ronchi P, Bragulat-Teixidor H, Tischer C, Gaspar I, Ephrussi A, Schwab Y, and Beck M (2019). Nuclear Pores Assemble from Nucleoporin Condensates During Oogenesis. Cell 179, 671–686.e17. 10.1016/j.cell.2019.09.022. [PubMed: 31626769]
69. Cochard A, Garcia-Jove Navarro M, Piroska L, Kashida S, Kress M, Weil D, and Gueroui Z (2022). RNA at the surface of phase-separated condensates impacts their size and number. Biophys. J 121, 1675–1690. 10.1016/j.bpj.2022.03.032. [PubMed: 35364105]

70. Hubstenberger A, Courel M, Bénard M, Souquere S, Ernoult-Lange M, Chouaib R, Yi Z, Morlot JB, Munier A, Fradet M, et al. (2017). P-Body Purification Reveals the Condensation of Repressed mRNA Regulons. Mol. Cell 68, 144–157.e5. 10.1016/j.molcel.2017.09.003. [PubMed: 28965817]
71. Su TT, Feger G, and O'Farrell PH (1996). Drosophila MCM protein complexes. Mol. Biol. Cell 7, 319–329. [PubMed: 8688561]
72. Grigoletto A, Lestienne P, and Rosenbaum J (2011). The multifaceted proteins Reptin and Pontin as major players in cancer. Biochim. Biophys. Acta 1815, 147–157. 10.1016/j.bbcan.2010.11.002. [PubMed: 21111787]
73. Ma W, and Mayr C (2018). A Membraneless Organelle Associated with the Endoplasmic Reticulum Enables 3'UTR-Mediated Protein-Protein Interactions. Cell 175, 1492–1506.e19. 10.1016/j.cell.2018.10.007. [PubMed: 30449617]
74. Lee JE, Cathey PI, Wu H, Parker R, and Voeltz GK (2020). Endoplasmic reticulum contact sites regulate the dynamics of membraneless organelles. Science 367, eaay7108. 10.1126/science.aay7108. [PubMed: 32001628]
75. Snead WT, Jalihal AP, Gerbich TM, Seim I, Hu Z, and Gladfelter AS (2022). Membrane surfaces regulate assembly of ribonucleoprotein condensates. Nat. Cell Biol 24, 461–470. 10.1038/s41556-022-00882-3. [PubMed: 35411085]
76. Phillips CM, and Updike DL (2022). Germ granules and gene regulation in the Caenorhabditis elegans germline. Genetics 220, iyab195, ARTN iyab195. 10.1093/genetics/iyab195. [PubMed: 35239965]
77. Pitt JN, Schisa JA, and Priess JR (2000). P granules in the germ cells of Caenorhabditis elegans adults are associated with clusters of nuclear pores and contain RNA. Dev. Biol 219, 315–333. 10.1006/dbio.2000.9607. [PubMed: 10694425]
78. Langerak S, Trombley A, Patterson JR, Leroux D, Couch A, Wood MP, and Schisa JA (2019). Remodeling of the endoplasmic reticulum in Caenorhabditis elegans oocytes is regulated by CGH-1. Genesis 57, e23267. 10.1002/dvg.23267. [PubMed: 30489010]
79. Patterson JR, Wood MP, and Schisa JA (2011). Assembly of RNP granules in stressed and aging oocytes requires nucleoporins and is coordinated with nuclear membrane blebbing. Dev. Biol 353, 173–185. 10.1016/j.ydbio.2011.02.028. [PubMed: 21382369]
80. Markussen FH, Michon AM, Breitwieser W, and Ephrussi A (1995). Translational control of oskar generates short OSK, the isoform that induces pole plasma assembly. Development 121, 3723–3732. 10.1242/dev.121.11.3723. [PubMed: 8582284]
81. Coutelis JB, and Ephrussi A (2007). Rab6 mediates membrane organization and determinant localization during Drosophila oogenesis. Development 134, 1419–1430. 10.1242/dev.02821. [PubMed: 17329360]
82. Tanaka T, and Nakamura A (2008). The endocytic pathway acts downstream of Oskar in Drosophila germ plasm assembly. Development 135, 1107–1117. 10.1242/dev.017293. [PubMed: 18272590]
83. Frise E, Hammonds AS, and Celniker SE (2010). Systematic image-driven analysis of the spatial Drosophila embryonic expression landscape. Mol. Syst. Biol 6, 345. 10.1038/msb.2009.102. [PubMed: 20087342]
84. Cinalli RM, Rangan P, and Lehmann R (2008). Germ cells are forever. Cell 132, 559–562. 10.1016/j.cell.2008.02.003. [PubMed: 18295574]
85. Hanyu-Nakamura K, Sonobe-Nojima H, Tanigawa A, Lasko P, and Nakamura A (2008). Drosophila Pgc protein inhibits P-TEFb recruitment to chromatin in primordial germ cells. Nature 451, 730–733. 10.1038/nature06498. [PubMed: 18200011]
86. Kina H, Yoshitani T, Hanyu-Nakamura K, and Nakamura A (2019). Rapid and efficient generation of GFP-knocked-in Drosophila by the CRISPR-Cas9-mediated genome editing. Dev. Growth Differ 61, 265–275. 10.1111/dgd.12607. [PubMed: 31037730]
87. Klattenhoff C, Bratu DP, McGinnis-Schultz N, Koppetsch BS, Cook HA, and Theurkauf WE (2007). Drosophila rasiRNA pathway mutations disrupt embryonic axis specification through activation of an ATR/Chk2 DNA damage response. Dev. Cell 12, 45–55. 10.1016/j.devcel.2006.12.001. [PubMed: 17199040]

88. Arkov AL, Wang JYS, Ramos A, and Lehmann R (2006). The role of Tudor domains in germline development and polar granule architecture. Development 133, 4053–4062. 10.1242/dev.02572. [PubMed: 16971472]

89. Lasko PF, and Ashburner M (1990). Posterior localization of vasa protein correlates with, but is not sufficient for, pole cell development. Genes Dev 4, 905–921. 10.1101/gad.4.6.905. [PubMed: 2384213]

90. Trcek T, Lionnet T, Shroff H, and Lehmann R (2017). mRNA quantification using single-molecule FISH in Drosophila embryos. Nat. Protoc 12, 1326–1348. 10.1038/nprot.2017.030. [PubMed: 28594816]

91. Lionnet T, Czaplinski K, Darzacq X, Shav-Tal Y, Wells AL, Chao JA, Park HY, de Turris V, Lopez-Jones M, and Singer RH (2011). A transgenic mouse for in vivo detection of endogenous labeled mRNA. Nat. Methods 8, 165–170. 10.1038/nmeth.1551. [PubMed: 21240280]

92. Schneider CA, Rasband WS, and Eliceiri KW (2012). NIH Image to ImageJ: 25 years of image analysis. Nat. Methods 9, 671–675. 10.1038/nmeth.2089. [PubMed: 22930834]

93. Bolte S, and Cordelières FP (2006). A guided tour into subcellular co-localization analysis in light microscopy. J. Microsc 224, 213–232. 10.1111/j.1365-2818.2006.01706.x. [PubMed: 17210054]

94. Jia D, Xu Q, Xie Q, Mio W, and Deng WM (2016). Automatic stage identification of Drosophila egg chamber based on DAPI images. Sci. Rep 6, 18850. 10.1038/srep18850. [PubMed: 26732176]

95. Foe VE, and Alberts BM (1983). Studies of nuclear and cytoplasmic behaviour during the five mitotic cycles that precede gastrulation in Drosophila embryogenesis. J. Cell Sci 61, 31–70. [PubMed: 6411748]

96. Morris LX, and Spradling AC (2011). Long-term live imaging provides new insight into stem cell regulation and germline-soma coordination in the Drosophila ovary. Development 138, 2207–2215. 10.1242/dev.065508. [PubMed: 21558370]

97. Teixeira D, Sheth U, Valencia-Sanchez MA, Brengues M, and Parker R (2005). Processing bodies require RNA for assembly and contain non-translating mRNAs. RNA 11, 371–382. 10.1261/rna.7258505. [PubMed: 15703442]

98. Dold A, Han H, Liu N, Hildebrandt A, Brüggemann M, Rücklé C, Hänel H, Busch A, Beli P, Zarnack K, et al. (2020). Makorin 1 controls embryonic patterning by alleviating Bruno1-mediated repression of oskar translation. PLoS Genet 16, e1008581. 10.1371/journal.pgen.1008581. [PubMed: 31978041]

Highlights

- The number, size, and distribution of germ granules is precisely regulated
- Oskar germ granules do not require RNA for their nucleation and stability
- RNA regulators and mitochondrial proteins control germ granule number and size
- ER, nuclear pore, and cytoskeletal proteins regulate germ granule distribution

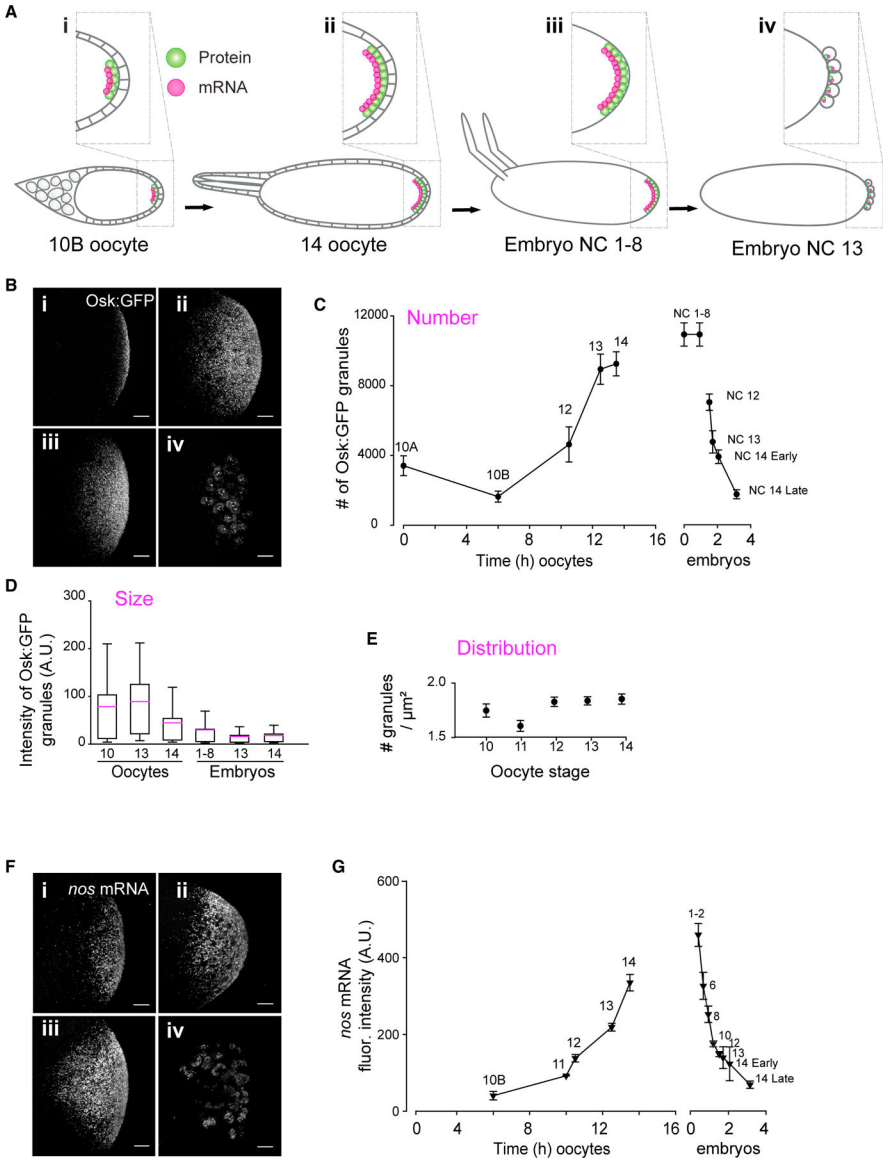

Figure 1. The number, size, and distribution of germ granules are precisely controlled

(A) (i–iv) Schematic of germ granule accumulation during development. NC, nuclear cycle.

(B and C) Accumulation of Osk:GFP in (i) stage 10 and (ii) stage 14 oocytes, and (iii) in NC 1–8 and (iv) NC 13 embryos. The numbers on the graph indicate oogenic stages and NCs. Mean ± SEM of 4–8 oocytes/stage and 2–14 embryos/NC.

(D) Total fluorescence intensity of Osk:GFP/granule. Magenta line marks the mean. All changes are statistically significant ($p < 0.001$; two-tailed t test).

(E) Number of Osk:GFP germ granules/μm^2. Mean ± SEM of 8–40 regions of interest (ROIs)/oocyte stage is shown. At least 20,000 germ granules from several oocytes and embryos/oogenic stage and NC were analyzed. Changes are not statistically significant (two-tailed t test).

(F) Accumulation of *nos* mRNA in (i) stage 10 and (ii) stage 14 oocytes, and (iii) in NC 1–8 and (iv) NC 13 embryos.

(G) Total fluorescence of *nos* mRNA. Mean ± SEM of 2–12 oocytes/stage or 3–13 embryos/group is shown. Scale bar, 10 μm.

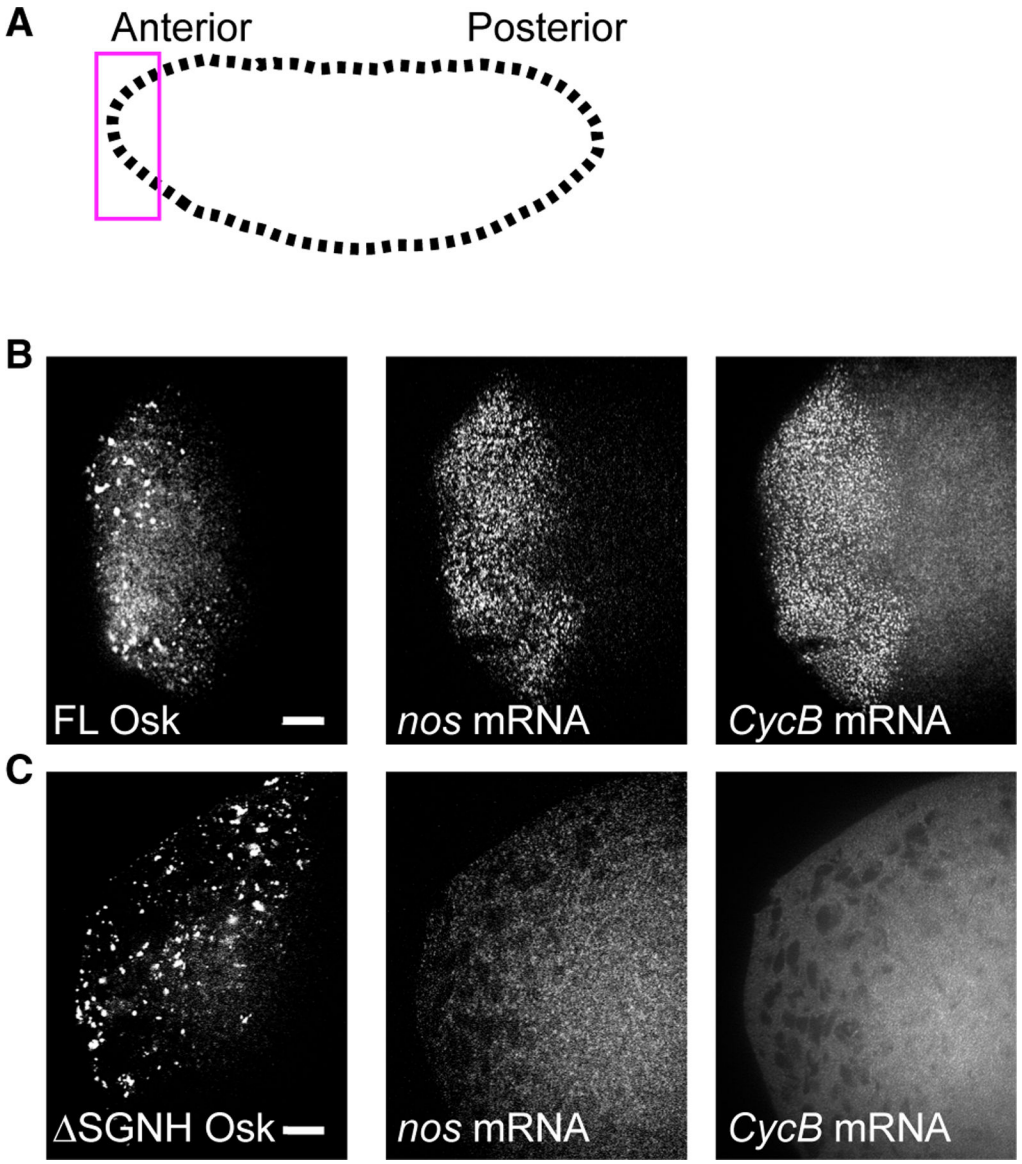

Figure 2. Osk-bound mRNAs are not required for condensation of Osk protein

(A) Depiction of embryonic poles.

(B and C) Embryos expressing the FL Osk:mCherry (B) or ΔSGNH Osk:mCherry (C) and labeled with probes against *nos* and *CycB*. Scale bar, 10 μm.

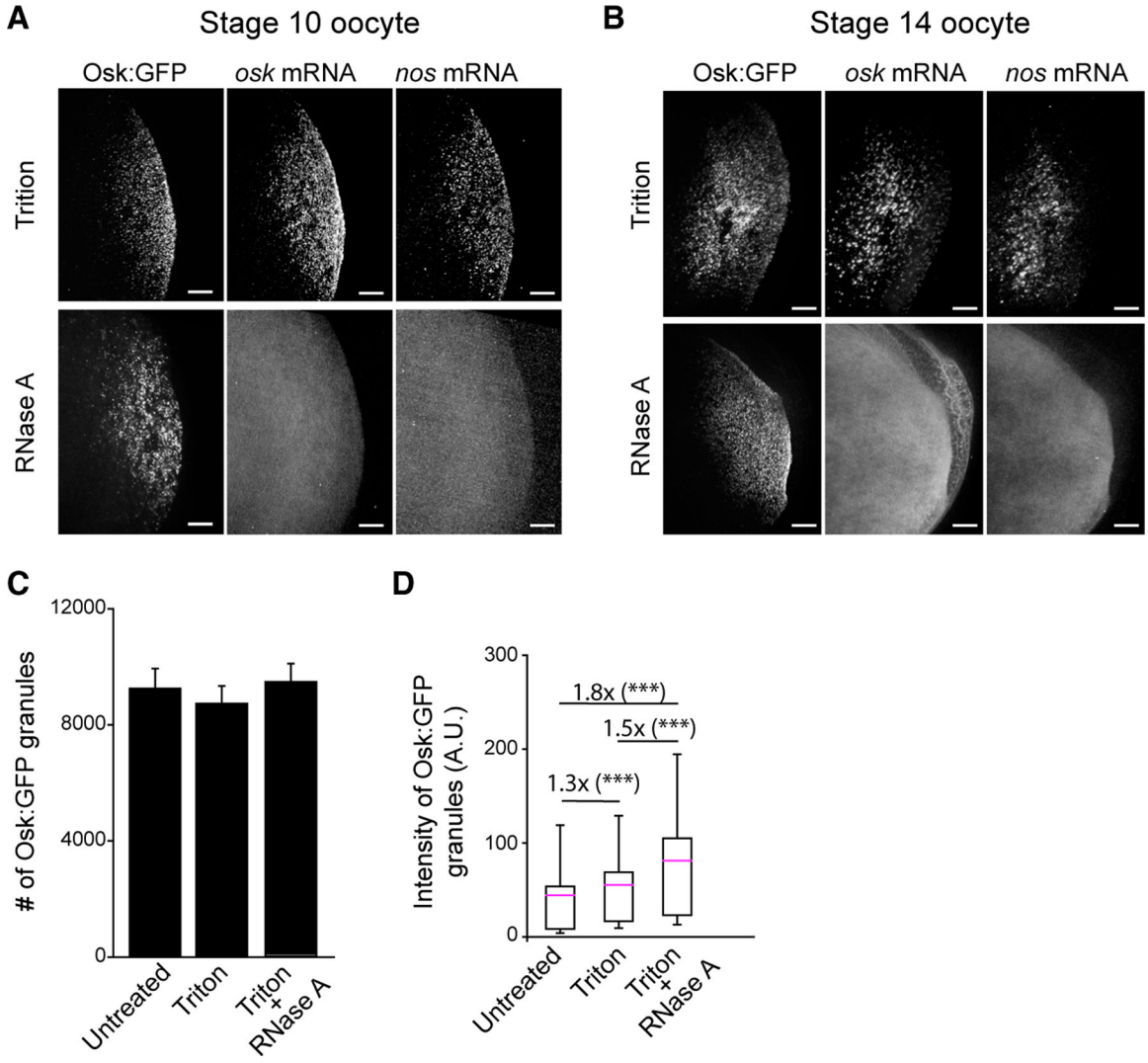

Figure 3. RNA is required for composition but not persistence of germ granules

(A and B) Stage 10 (A) and stage 14 (B) oocytes expressing Osk:GFP germ granules were treated with 1% Triton X-100 (control) or Triton X-100 followed by RNase A and hybridized with probes against *osk* and *nos*.

(C) Number of Osk:GFP granules in stage 14 oocytes untreated (from Figure 1C), treated with Triton X-100 only, or treated with Triton X-100 and RNase A. Mean ± SEM of 4–−8 oocytes/condition is shown.

(D) Total fluorescence intensity of Osk:GFP/granule in stage 14 oocytes that were untreated (data from Figure 1D), treated with Triton X-100 only, or treated with Triton X-100 and RNase A. Mean ± SD of at least 34,946 germ granules from four stage 14 oocytes is shown. ***$p < 0.001$ (two-tailed t test). Scale bar, 10 μm.

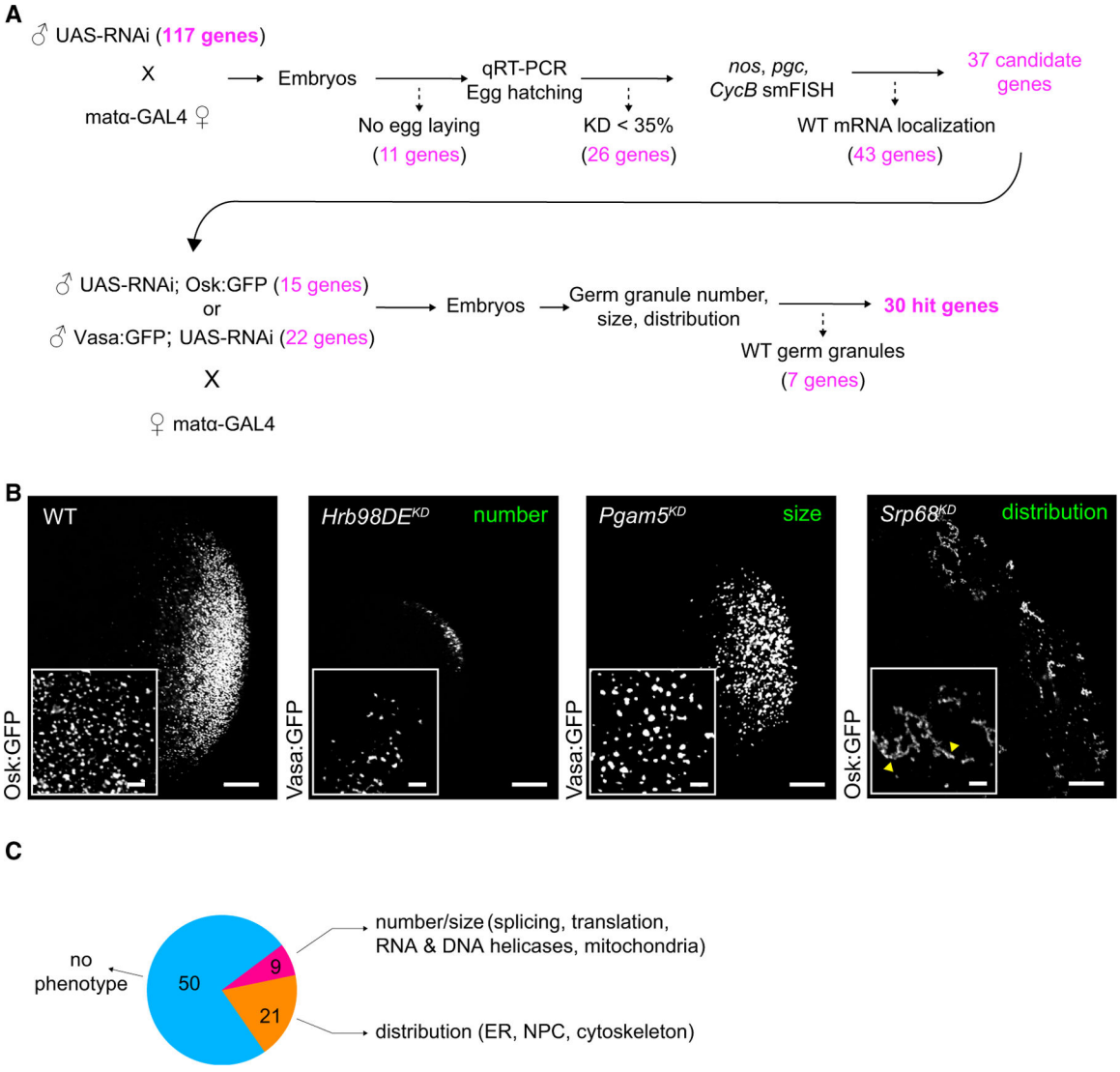

Figure 4. RNAi screen identifies regulators of germ granule number, size, and distribution

(A) Design of the RNAi screen.

(B) Embryos with an altered number (*Hrb98DE*), size (*Pgam5*), or distribution (*Srp68*) of germ granules. Yellow arrowheads point at germ granules with a branched distribution.

(C) Genes that alter the number, size, and distribution of germ granules. Scale bar, 2 μm (small images), 10 μm (larger images).

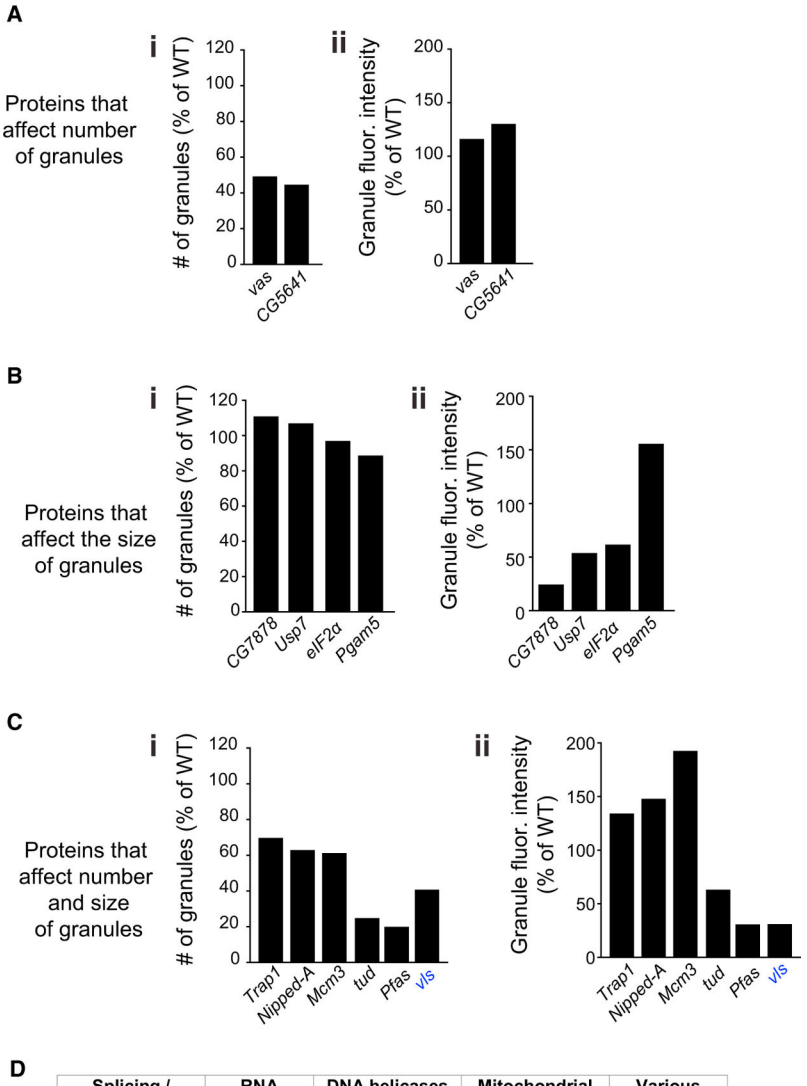

D

Splicing / translation	RNA helicases	DNA helicases / repair	Mitochondrial protein	Various
CG5641, *eIF2α*	*vas*, *CG7878*	*Mcm3*, *Nipped-A*	*Trap1*, *Pgam5*	*tud*,*Usp7*, *Pfas*

Figure 5. RNA regulators, helicases, and mitochondria proteins control germ granule number and size

(A–D) Proteins that regulate germ granule number (A), size (B), number and size (C), and their functional categorization (D). *vls* (blue) did not co-purify with Osk[51] but is a known regulator of germ plasm assembly[54] and was included for comparison.

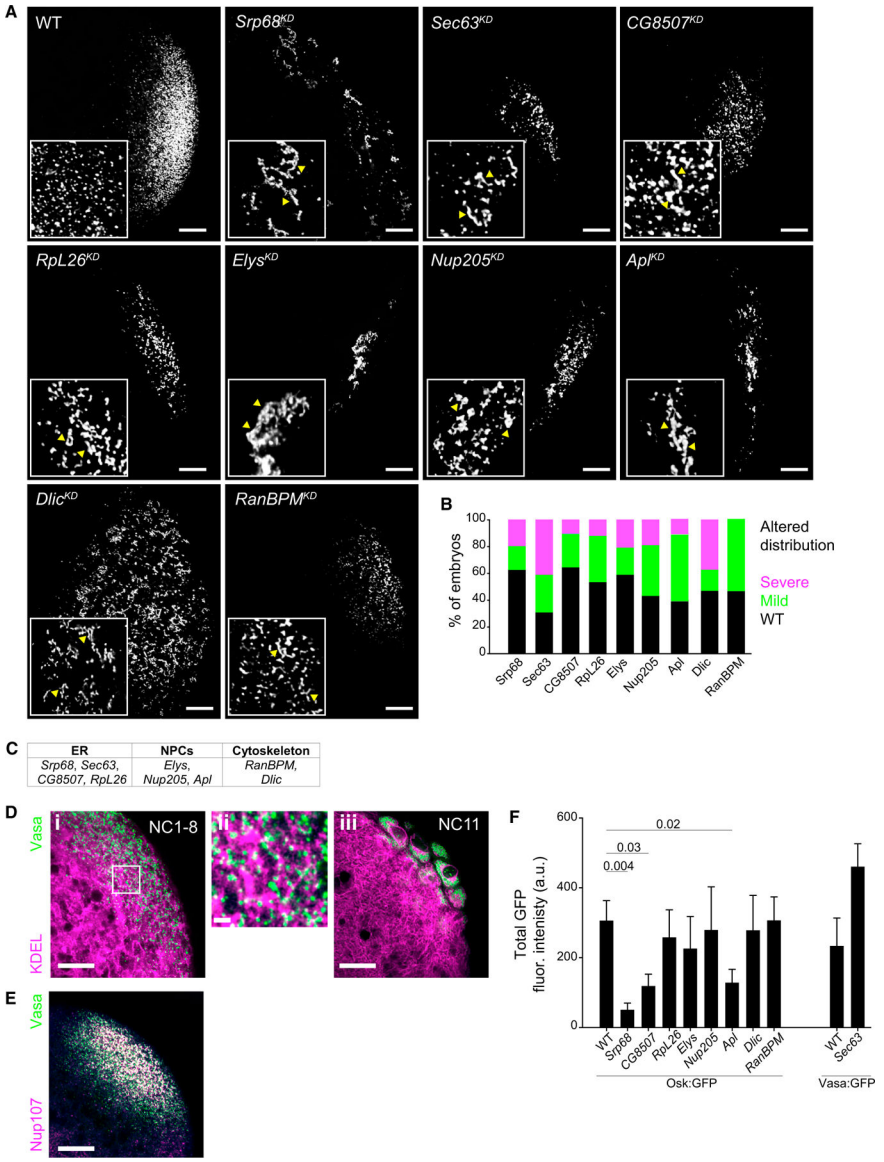

Figure 6. Proteins of the ER, NPC, and cytoskeleton regulate the distribution of germ granules

(A) Osk:GFP or Vasa:GFP germ granules in WT embryos and in embryos upon RNAi-induced KD. Yellow arrowheads point at germ granules with a branched distribution. Image of the *Srp68*^{KD} embryo is from Figure 4.

(B) Embryos with severe, mild, and WT germ granule distribution.

(C) Gene Ontology (GO) analysis of gene hits.

(D) (i–iii) Germ granules (green) co-localize with the ER (RFP-KDEL, magenta).

(E) Germ granules (green) co-localize with the NPCs (magenta).

(F) Intensity of Osk:GFP and Vasa:GFP germ granules upon RNAi-induced KD. Mean ± SEM of 7–23 embryos/gene is shown. Statistical significance: two-tailed t test. Scale bar, 1 μm in (D ii); 10 μm in (A), (D i), (D iii), and (E).

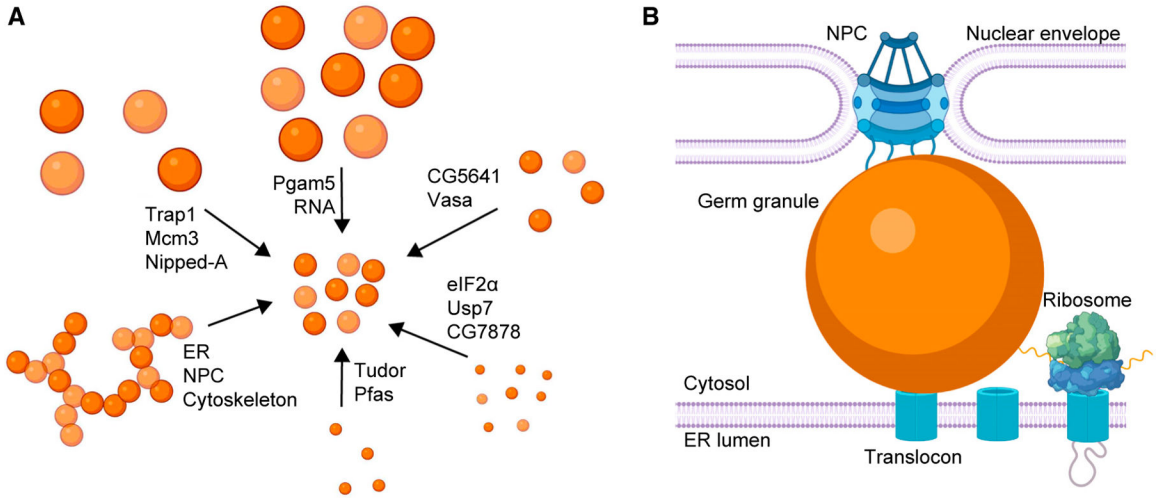

Figure 7. Regulation of germ granules by their mRNAs and proteins

(A) Regulators of germ granule number, size, and distribution.

(B) Anchoring of germ granules to the ER and NPCs.

KEY RESOURCES TABLE

REAGENT or RESOURCE	SOURCE	IDENTIFIER
Antibodies		
Polyclonal rabbit Vasa antisera	Gift from Ruth Lehmann lab	RRID:AB_2940894
Goat anti-rabbit Alexa Fluor 546	Invitrogen	A–11035
Chemicals, peptides, and recombinant proteins		
20% Paraformaldehyde Aqueous Solution, EM Grade	Electron Microscopy Sciences	15713
Schneider's Drosophila Medium	Thermo Fisher Scientific	21720024
Methanol	Fisher chemical	A412–4
10% Fetal Bovine Serum	Invitrogen	10082–139
Penicillin-streptomycin	Fisher	15140122
Insulin	Sigma-Aldrich	I5500–500MG
Triton X-100	Sigma-Aldrich	T8787–250ML
RNase A TRIzol reagent	Millipore Sigma	10109169001
TRIzol reagent	Thermo Fisher Scientific	15596026
β-mercaptoethanol	Millipore Sigma	444203–250ML
protease inhibitor complete mini EDTA free	Sigma-Aldrich	11836170001
RNase Out	Invitrogen	10777019
2X RNA Loading Dye	NEB	N0362
RQ1 RNase-Free DNase	Promega	M6101
Oligo dT(20) primer	Thermo Fisher Scientific	18418020
Critical commercial assays		
SuperScript® IV Reverse Transcriptase	Invitrogen	18090010
SYBR Green reporter dye	Thermo Fisher Scientific	4309155
Direct-zol Microprep RNA Kit	Zymo Research	R2061
Experimental models: Organisms/strains		
w1118 (''wild type'')	BDSC	5905
Vasa:GFP transgene	Trcek et al.[44]	N/A
Osk:EGFP (CRISPR/Cas9)	Gift from Graydon Gonsalvez lab	N/A
Vasa:EGFP (CRISPR/Cas9)	Kina et al.[86]	N/A
Tud:EGFP (CRISPR/Cas9)	Kina et al.[86]	N/A
Aub:EGFP (CRISPR/Cas9)	Kina et al.[86]	N/A
Vasa:mCherry (CRISPR/Cas9)	Kina et al.[86]	N/A
Matα-gal4; matα-gal4	Gift from Ruth Lehmann lab	N/A
mnk aub^{HN2}	Klattenhoff et al.[87]	N/A
mnk, aubQC42	Klattenhoff et al.[87]	N/A
TudC30–51	Arkov et al.[88]	N/A
tud1	Arkov et al.[88]	N/A

REAGENT or RESOURCE	SOURCE	IDENTIFIER
vasD1	Lasko et al.[89]	N/A
vas1	BDSC	1574
Nup107:GFP	BDSC	35514
RFP-KDEL	BDSC	30909
FL-Short Osk:mCherry	Hurd et al.[51]	N/A
ΔSGNH Short Osk:mCherry	Hurd et al.[51]	N/A
RNAi lines are listed in Table S2	VDRC/BDSC	Table S2
Oligonucleotides		
osk smFISH probes	Trcek et al.[44]	N/A
nos smFISH probes	Trcek et al.[44]	N/A
CycB smFISH probes	Trcek et al.[44]	N/A
gcl smFISH probes	Trcek et al.[44]	N/A
pgc smFISH probes	Trcek et al.[44]	N/A
ftz smFISH probes (Table S4)	Stellaris smFISH probes	N/A
The list of all qRT-PCR primers used in this study are reported in Table S3	IDT Technologies	N/A
Software and algorithms		
Airlocalize spot detection algorithm	Trcek et al.; Lionnet et al.[90,91]	N/A
SigmaPlot	www.systatsoftware.com	N/A
ImageJ	Schneider et al.[92]	https://imagej.nih.gov/ij/
PCC(Costes) co-localization ImageJ plugin	Bolte et al.[93]	JACoP ImageJ
Huygens deconvolution software	SVI	N/A
Other		
Hard-Shell 96 well qRT-PCR plates	Bio Rad	HSP9601
Lab-Tek II 8 Chambered Coverglass dish	Thermo Fisher Scientific	155409PK
CFX Opus 96 Real-Time PCR System	Bio Rad	N/A
Vt-iSIM	BioVision Technologies	N/A
Hard-Shell 96 well qRT-PCR plates	Bio Rad	HSP9601